ELSEVIER

Journal of Volcanology and Geothermal Research 83 (1998) 241–267

Journal of volcanology and geothermal research

Computer-simulation models of scoria cone degradation

Donald M. Hooper *, Michael F. Sheridan

Department of Geology, 876 Natural Sciences and Mathematics Complex, Box 603050, State University of New York at Buffalo, Buffalo, NY 14260-3050, USA

Received 30 August 1997; accepted 9 March 1998

Abstract

Long-term erosional modifications of the relatively simple morphology of scoria ('cinder') cones are ideally suited for study by field and computer-simulation methods. A series of temporally-distinct cones in the San Francisco and Springerville volcanic fields of Arizona provides the foundation for documenting the degradational evolution of scoria cones in a semi-arid climate. Progressive changes due to erosion are illustrated by the systematic decrease with increasing age of various morphometric parameters, including scoria cone height, cone height/width ratio (H_{co}/W_{co}), crater depth/width ratio, and slope angle. For example, Holocene–latest Pleistocene cones in the San Francisco field have a mean H_{co}/W_{co} value of 0.178 ± 0.041, a mean maximum slope angle of $29.7 \pm 4.2°$, and a mean average slope angle of $26.4 \pm 7.3°$, whereas the group of Pliocene cones have values of 0.077 ± 0.024, $20.5 \pm 5.8°$, and $8.7 \pm 2.7°$, respectively. Comparative morphology of scoria cones is a potentially useful dating tool for mapping volcanic fields.

In order to better understand the degradational modifications of these volcanic landforms, we have developed a numerical approach to simulate the surficial processes responsible for the erosion of a typical scoria cone. The simulation algorithm can apply either a linear diffusion-equation model or a model with a nonlinear transport law. Using a finite-difference formulation, the simulation operates upon a three-dimensional scoria cone input as a matrix of elevation values. Utilizing both field and model results, the correlation between changing H_{co}/W_{co} value, cone age, and computer time step was expressed graphically to derive comprehensive values of the transport or diffusion coefficient (D_f) for both volcanic fields. For the San Francisco volcanic field, D_f had a calculated value of 21.4 m^2/kyr for the linear model and 5.3 m/kyr for the nonlinear model, while for the Springerville volcanic field D_f had a calculated value of 24.4 m^2/kyr for the linear model and 6.3 m/kyr for the nonlinear model.

Keywords: computer simulation; San Francisco volcanic field; Springerville volcanic field; scoria cones; cinder cones; diffusion; geomorphological models; numerical simulation; surficial processes

1. Introduction

Most scoria cones (also known as cinder cones) are conical structures of ballistically-ejected fragments topped by a bowl-shaped crater. These small volcanoes are usually similar in structure and composition, and often cluster by the dozens or even hundreds in volcanic fields or on the flanks of larger volcanoes. They may be the most common volcanic landform (Wood, 1980a,b). The degradational evolution of these cones can be correlated with the length of time they have been exposed to erosion. The

* Corresponding author. Tel.: +1-716-645-6800 ext. 6100; fax: +1-716-645-3999; e-mail: dhooper@acsu.buffalo.edu

0377-0273/98/$19.00
PII S0377-0273(98)00031-6

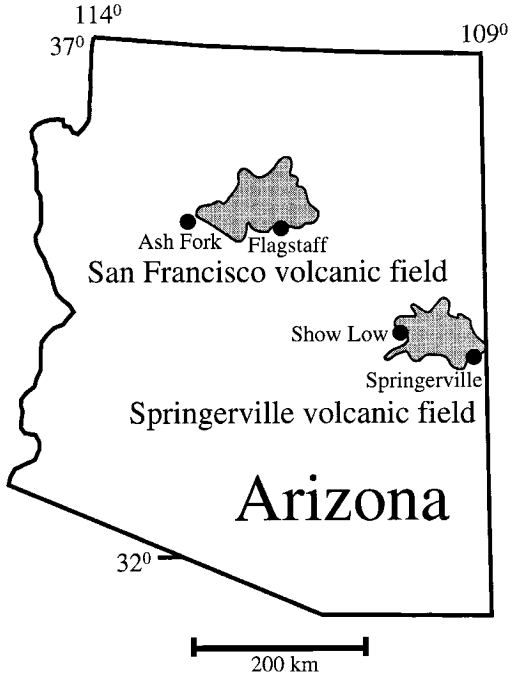

Fig. 1. Location of the San Francisco and Springerville volcanic fields, AZ (USA). Outlines of the fields are from Moore and Wolfe (1987), Newhall et al. (1987), Ulrich and Bailey (1987), and Wolfe et al. (1987a,b) for the San Francisco field and from Condit et al. (1989) and Condit (1991) for the Springerville field.

progressive decrease in cone height (H_{co}), cone height/width ratio (H_{co}/W_{co}), and slope angle with increasing age is the basis for relative dating of cones by comparative measurements. Extensive fieldwork and topographic map measurements were conducted to quantitatively document the morphometric changes associated with the erosional modification of scoria cones. The San Francisco and Springerville volcanic fields of Arizona (Fig. 1) were the primary focus of this research because of their accessibility, the publication of topographic and geologic maps, and the availability of a temporally-distinct population of scoria cones dated by a variety of radiometric or other chronometric techniques. Examples of typical erosional modifications are illustrated in Fig. 2.

We have also chosen a numerical approach to aid our study of the changing morphology of these volcanic landforms. Linear and nonlinear diffusion-

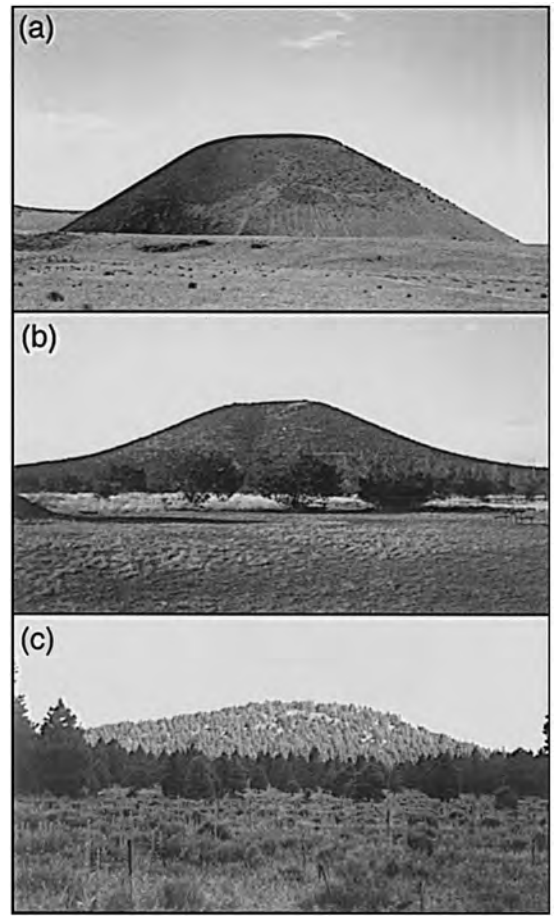

Fig. 2. These photographs illustrate three examples in the progressive pattern of scoria cone erosion in the San Francisco volcanic field, AZ. (a) SP Mountain (V5703) is a 250-m-high cone that has been dated at 71,000±4000 yr (Baksi, 1974). As is typical for 'youthful' cones, it has steep slopes, a high H_{co}/W_{co} value, and a bowl-shaped crater with a sharp rim (not visible). View is to the west. (b) This unnamed cone (V3202) belongs to the early Pleistocene–late Pliocene age group. This view to the north displays a profile that is more subdued than that for younger cones. The cone no longer has a crater, but does have an extensive debris apron. (c) Unnamed cone (V2320) photographed looking northeast. This cone is Pliocene in age and has been degraded to a shield-like hill with low slope angles. The location of each scoria cone (vent or sample site) in the San Francisco field (and also adopted for the Springerville field) is identified by a four-digit numbering system, as established by Moore and Wolfe (1987), Newhall et al. (1987), Ulrich and Bailey (1987), and Wolfe et al. (1987a,b). The first digit of the vent number represents the township (second digit of the township number), the second digit represents the range, and the last two digits are the section number in which the site is located. Therefore, cone (or vent) number V5703 is in T.25N., R.7E., Section 3.

equation models have been used to simulate the slope processes that are responsible for the erosion of a variety of landforms (e.g., Culling, 1960; Hirano, 1968; Hanks et al., 1984; Nash, 1984; Andrews and Bucknam, 1987; Bursik, 1991). The relatively simple morphology and internal structure of scoria cones is ideally suited for the study of their long-term degradation by a diffusion-equation method because they form rapidly and their original morphometric parameters can be estimated with a reasonably high degree of certainty compared to many other landforms. On a macroscopic scale in a geomorphologic system, diffusion is the process by which matter (e.g., soil, rock fragments, cinders) is transported by random movements from one part of the system to another driven by a potential field, in this case elevation.

Incorporating the diffusion-equation method, a computer model has been developed to simulate the degradational evolution of scoria cones. This model can utilize either a linear or a nonlinear diffusion-equation algorithm expressed in finite-difference form to operate upon a three-dimensional scoria cone input as a matrix of elevation values. The linear version of the model assumes that downslope movement is directly proportional to surface gradient to the first power and simulates erosion by rainsplash (raindrop impact), soil creep, freeze–thaw movement, and bioturbation. Mathematically more complex, a nonlinear version of the model was developed to address overland flow or slope wash processes. Therefore, the simple dissection of cone flanks by intermittent gully processes can be simulated by a second version of the numerical model that accommodates slope wash with gullying. Computer simulation is an efficient methodology for modeling three-dimensional landform modification under a variety of assumptions, conditions, and cases. It is our objective to combine both field-based research and numerical modeling in the study of the degradational changes of these volcanic landforms.

2. Previous research

Using a diagnostic scheme he first published in 1936, Colton (1967) classified the basaltic flows and scoria cones of the San Francisco volcanic field, AZ, into five stages based upon degree of comparative degradation and weathering (oxidation of fragmentary material). This may represent the first examination of the degradational changes over time of a series of scoria cones. Segerstrom (1950, 1960, 1966) studied in great detail the erosion of the historically active (1943 to 1952) Parícutin scoria cone in the Michoacán-Guanajuato volcanic field of Mexico. He noted that rill erosion had not started on the sides of the cone and that the tephra was still too coarse and permeable to permit surface flow of rainwater. He further observed that the ash mantle covering both the cone and surrounding terrain is gradually being removed by raindrop splash, sheet wash, landsliding, channel erosion, and deflation by wind. Porter (1972) contributed one of the first studies to quantify the relationships between the various morphometric parameters of scoria cones. He examined the morphology, distribution, and size frequency of the cones on Mauna Kea, HI.

A few authors have employed comparative morphology of scoria cones within a chosen volcanic field to establish a relative-age scheme or a relative-age scheme supplemented by chronometric dates. Scott and Trask (1971) employed the maximum cone slope angle and the ratio of cone radius/cone height to derive the relative morphologic ages for 15 cones in the Lunar Crater volcanic field, NV. Bloomfield (1975) studied the morphology of scoria cones as well as lava flows in the Chichináutzin volcanic field of central Mexico. By using morphologic parameters, he devised a calibration scheme from radiocarbon dates of charcoal and paleosols to establish the relative ages for 41 cones in this late Quaternary field. Martin del Pozzo (1982) later determined the geomorphologic parameters and relative-age assignments for 146 cones in a different region of the same volcanic field.

Wood (1980b) made extensive measurements of the geometry of scoria cones to conclude that it is possible to roughly date cones by simple measurements of morphology. He also used simple models to quantify cone degradation by erosion and mass wasting of material from cone flanks by subsequent lava flows. He stressed the importance of climate on cone erosion and that a study of cone morphology may provide information on past climates.

Other studies of scoria cone morphology include Luhr and Carmichael (1981) who examined 11 late Quaternary cones of the Colima volcanic complex, Mexico, and devised a preliminary estimation of their ages by comparing averaged maximum slope angles. By utilizing morphologic parameters and radiocarbon dates of seven scoria cones in the Michoacán-Guanajuato volcanic field of central Mexico, Hasenaka and Carmichael (1985a,b) classified 78 of approximately 900 cones to be younger than 40,000 yr B.P. In a detailed geomorphologic study, Dohrenwend et al. (1986) used K–Ar analyses to date 11 cones in the Cima volcanic field, CA, and provided an example of scoria cone degradation under the current arid conditions of the Mojave Desert. Examining the same group of cones, Renault (1989) concluded that debris-flow, fluvial, and colluvial processes are the principal mechanisms by which these cones degrade through time.

3. Geologic setting

In order to quantitatively document the erosional modifications of scoria cones, fieldwork was conducted in the San Francisco and Springerville volcanic fields of Arizona. The San Francisco volcanic field consists of late Miocene to Holocene volcanic rocks resting upon Permian and Triassic sedimentary deposits. The field extends approximately 110 km east–west and 70 km north–south (Fig. 3). Previous researchers have identified more than 600 volcanoes with their associated lava or pyroclastic flows (Robinson, 1913; Cooley, 1962; Hodges, 1962; Breed, 1964; Colton, 1967; Damon et al., 1974; Moore et al., 1974, 1976). San Francisco Mountain, the remnants of a large stratovolcano rising to an elevation of 3850 m a.s.l. (above sea level), is the dominant physiographic and volcanic feature in this field. Sunset Crater and its associated eruptive prod-

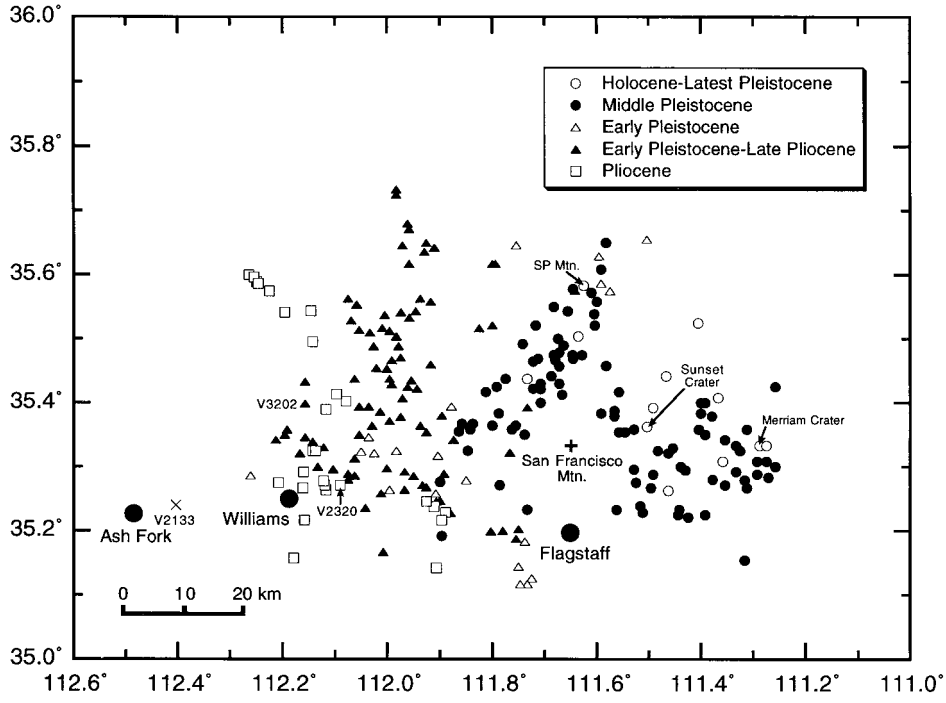

Fig. 3. Distribution of the 237 scoria cones used in the morphometric analyses of the San Francisco volcanic field, AZ. San Francisco Mountain is a stratovolcano composed of andesitic flows with dacitic and rhyolitic domes and flows. Scoria cones mentioned in the text are labeled. Also shown near the city of Ash Fork is V2133, a Miocene–early Pliocene cone belonging to the informal 'rim basalts' group of volcanic rocks that pre-date the San Francisco volcanic field.

ucts are the youngest volcanic features in the region. On the basis of dendrochronology, Smiley (1958) determined that the eruption at Sunset Crater commenced A.D. 1064/1065. Cone distribution shows an eastward migration of volcanism, as previously identified by Luedke and Smith (1978) and Tanaka et al. (1986). Although volcanic landforms with a basaltic composition are dominant, several intermediate to silicic volcanic centers have been recognized.

In 1976 the U.S. Geological Survey began a geothermal research program to study the San Francisco field. The remanent magnetism of volcanic rocks was determined for over 650 sites in the field (Tanaka et al., 1986, 1990). In addition to the polarity of remanent magnetization, they examined K–Ar ages, spatial and petrographic associations, stratigraphic relationships, and the state of preservation of lava flows and scoria cones. These data were compiled into five 1:50,000-scale geologic maps covering the San Francisco volcanic field: Moore and Wolfe (1987), Newhall et al. (1987), Ulrich and Bailey (1987), and Wolfe et al. (1987a,b). Prior to this research program, Moore and Wolfe (1976) had published a geologic map of the eastern region of the volcanic field. Collectively these maps provided the chronostratigraphic units necessary for identifying volcanic deposits, landforms, and cone age groups.

Approximately 400 volcanic vents have been identified in the Springerville volcanic field, but it does not contain silicic centers, high-silica flows, or large composite volcanoes (Condit et al., 1989; Connor et al., 1992). Most vent structures are scoria cones, but there are also spatter cones, maar craters, fissure vents, and small shield volcanoes. Our investigation only concentrates upon the scoria cones from each field (Fig. 4). A geologic map has been completed for the western part of the field (Condit, 1991), and another covers the entire field (Condit et al., in press). A dynamic digital (CD-ROM) version of the map of the entire field is also available (Condit, 1995). Radiometric and chronostratigraphic data are available in both Condit (1995) and Condit et al. (in press). These data and maps show that

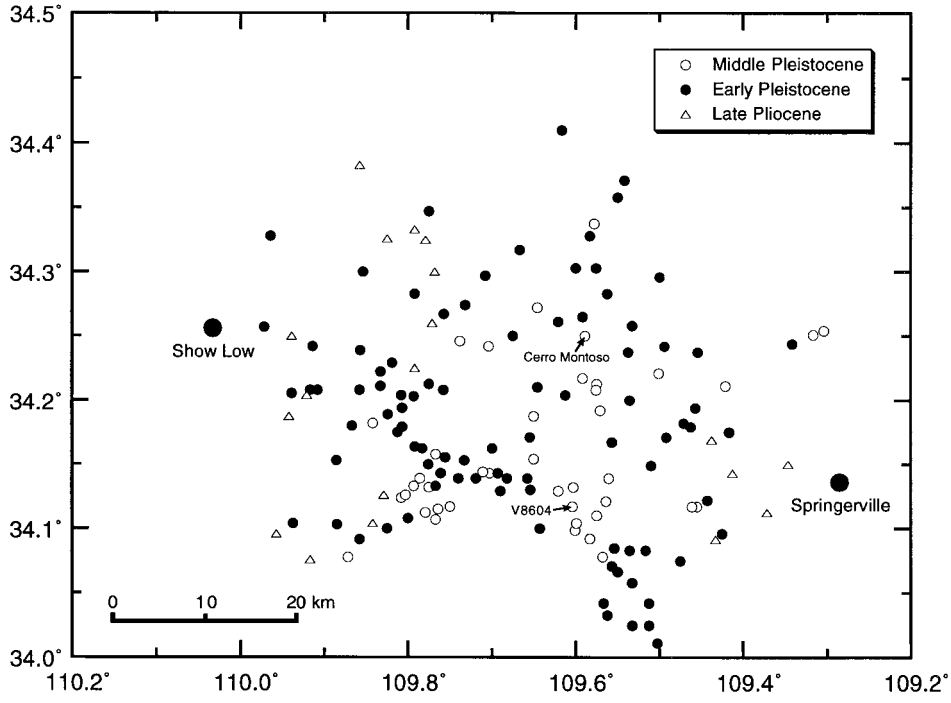

Fig. 4. Distribution of the 152 scoria cones used in the morphometric analyses of the Springerville volcanic field, AZ. Cerro Montoso (V0621A) is the largest scoria cone in this field with a calculated height (H_{co}) of 286 m. Cones mentioned in the text are labeled.

although some older volcanic materials have been buried, most of the volcanic units range from 0.3 to 2.1 m.y. A study of the recurrence rates of volcanism in the Springerville field by Condit and Connor (1996) revealed a shift in the locus of magmatism from west to east, but this trend is not as well-defined as in the San Francisco field.

Both volcanic fields are situated on the southern margin of the Colorado Plateau. The climate over most of the region is semi-arid, supporting pine forests at higher elevations and pinyon-sagebrush communities at lower elevations where precipitation amounts are lower. The Springerville field has a higher average elevation. This was determined by measuring the average basal elevation for each of the 152 scoria cones for which detailed morphometry was calculated. These cones had an average basal elevation of 2293 m a.s.l. (7524 ft) compared to 2076 m a.s.l. (6811 ft) for the 237 cones with detailed morphometric measurements in the San Francisco field.

Mean annual precipitation, which increases with elevation, is approximately 500 mm in Flagstaff (at an elevation of 2135 m a.s.l.) (Sellers and Hill, 1974). A network of climatological stations has allowed Sellers and Hill (1974) to plot average annual precipitation contours, which show that the area encompassed by each volcanic field receives between 15 in. (381 mm) and 25 in. (635 mm) of precipitation annually.

Sellers and Hill (1974) also provide a comprehensive treatment of the climate of Arizona, some of which is summarized here. From early July until early September, afternoon thunderstorms develop almost daily over the higher terrains. These convective storms are usually short-lived and are triggered by moist, tropical air flowing into Arizona from the Gulf of Mexico. Additional precipitation is provided by winter frontal storms that enter the state from the west after picking up moisture from the Pacific Ocean. Most of this precipitation falls as snow.

4. Methods of geomorphologic analysis

Morphology and morphometry were determined from topographic maps, field measurements, field photographs, and aerial photographs. The topographic maps (Department of the Interior, U.S. Geological Survey) have a scale of 1:24,000 and usually a contour interval of 20 ft ($\approx$ 6 m). Field measurements were made by standard surveying techniques. In addition, this data base was supplemented by U.S. Geological Survey Digital Elevation Models (DEMs).

Cone height (H_{co}) is defined as the difference between average basal elevation and maximum crater rim or summit elevation. Cone width or basal diameter (W_{co}) is calculated as the average of the maximum and minimum basal diameters for each cone. This is essentially the same methodology described by Settle (1979) and employed by other researchers, including Hasenaka and Carmichael (1985a,b). The debris apron is incorporated in W_{co}, although the extent of the debris apron may become harder to recognize in older cones as it mixes with Quaternary alluvial deposits. (A constant volume was maintained in our numerical simulations until material reached the cells at the margin of the finite-difference grid when it was removed at a rate proportional to material entering the (kernel) cell to avoid artificial accumulation of material along grid margins.) Cone width increases due to debris apron growth, but the apron will gradually slow in its rate of growth and then undergo a reduction in size as it also experiences erosion (Dohrenwend et al., 1986). When lacking field inspection, the spacing and inflections of contour lines on the topographic maps offer a reasonable measure of the margins of a cone. The H_{co}/W_{co} ratio decreases with an increase in age as erosion diminishes cone height by transporting material to debris aprons surrounding the cone base.

Crater width or diameter (W_{cr}) is defined as the average of the maximum and minimum diameters of the crater. Crater depth (D_{cr}) is designated as the difference between maximum rim or summit elevation and the lowest elevation in the crater.

Although this research will focus most heavily upon H_{co}/W_{co} values, the decrease in the maximum cone slope angle with an increase in age provides another comparative morphometric measurement by which to establish the relative ages of scoria cones. Maximum cone slope angles can be measured in the field, taken from aerial or field photographs (Ray, 1960), or determined from the spacing of contour lines on topographic maps. For most scoria cones,

the maximum slope angle of unconsolidated lapilli, cinders, and bombs is greatest when they are first deposited. Erosional processes thereafter transport material from the upper portion of the cone to debris aprons and also into the crater itself. This advancement of erosion produces a gradual decrease in both the average and maximum slope angle with time as the cone becomes more rounded and the debris aprons increase in size around the base and lower flanks. Downslope transport degrades the cone so that the maximum slope angle is less than the angle of repose of the initial cone. Scott and Trask (1971) were the first to identify the usefulness of this parameter for deriving relative cone ages.

Another indicator of changing morphology with time is the average slope angle. For cones still retaining a crater, the average cone slope angle (S_{ave}) is defined by:

$$S_{ave} = \tan^{-1}\left[2H_{co}/(W_{co} - W_{cr})\right] \quad (1a)$$

where H_{co} is cone height, W_{co} is cone width or diameter, and W_{cr} is crater width or diameter. This is the same equation used by Hasenaka and Carmichael (1985b).

For older cones that have lost the crater to erosion, the average slope angle can be calculated by:

$$S_{ave} = \tan^{-1}\left[2H_{co}/W_{co}\right] \quad (1b)$$

As consistent as measurements of these morphometric parameters may be, there will always be a subjective element that introduces errors when making these determinations. We agree with the estimate of Dohrenwend et al. (1986) that measured values of the various morphometric parameters probably have an uncertainty of ± 10 to 15%.

5. Field and map analysis of cone degradation

For morphometric and degradational analysis, scoria cones of the San Francisco volcanic field were grouped into five age categories based on the available geologic maps (Moore and Wolfe, 1987; Newhall et al., 1987; Ulrich and Bailey, 1987; Wolfe et al., 1987a,b) and the affiliated chronometric data also listed in companion publications (Tanaka et al., 1986, 1990). From youngest to oldest their age groups were: Holocene–latest Pleistocene (0 to 0.16 m.y.), middle Pleistocene (0.16 to 0.73 m.y.), early Pleistocene (0.73 to 2.0 m.y.), early Pleistocene–late Pliocene (mostly 2.0 to 2.48 m.y., but including some cones mapped in a broad unit of 0.73 to 2.48 m.y.), and Pliocene (2.48 to 5.0 m.y.). Since remanent magnetism was determined for over 650 sites, their sampling was comprehensive. They report that polarity-chronostratigraphic assignments were made for all eruptive units represented by basaltic vents, for most of the lava flows, and for most intermediate to silicic volcanic units. However, some basaltic rocks having stratigraphic positions near polarity chronozone boundaries could not be placed with certainty into a specific polarity chronozone. This resulted in several (usually older) scoria cones having a poorly-defined age assignment that was not acceptable for analysis. The age categories are not necessarily consistent with established age classifications and are strongly influenced by three magnetopolarity sequences: Bruhnes Normal-Polarity Chronozone (0.73 m.y. to present), Matuyama Reversed-Polarity Chronozone (2.48 to 0.73 m.y.), and the pre-Matuyama Chronozone (about 5.0 to 2.48 m.y.).

Three hundred and ninety scoria cones were counted in the San Francisco volcanic field, although the actual number remains somewhat uncertain since some of these volcanic landforms could have been misclassified. The final statistical analysis included just 237 of these cones for reasons that will be explained below. For example, morphometry was actually measured for an additional 28 cones, but they could not be placed with certainty into one of the five age groups because their assigned ages were too broad. These cones were later given relative ages (Hooper, 1994). Also deleted from the final analysis was an assortment of 78 cones from the various age groups. Maximum slope angle measurements were made for these cones, but their complete morphometry could not be calculated because of either a severe elongation in one direction, extensive breaching, multiple vents, or a poorly-defined cone base.

A small number of conical landforms less than about 30 m high was excluded from the geomorphologic analysis because they could not be distinguished with confidence from spatter cones. Some of these small cones may represent vents that did not

Table 1
Major morphometric parameters for cone age groups in the San Francisco volcanic field, AZ

Cone age group	n	Mean H_{co}/W_{co} ($\pm 1\ \sigma$)	Mean maximum slope angle ($\pm 1\ \sigma$)	Mean average slope angle ($\pm 1\ \sigma$)
Holocene–Latest Pleistocene (0–0.16 m.y.)	12	0.178 ± 0.041	$29.7 \pm 4.2°$	$26.4 \pm 7.3°$
Middle Pleistocene (0.16–0.73 m.y.)	91	0.135 ± 0.028	$25.4 \pm 3.7°$	$18.1 \pm 4.9°$
Early Pleistocene (0.73–2.0 m.y.)	20	0.113 ± 0.027	$23.6 \pm 4.8°$	$13.4 \pm 3.2°$
Early Pleistocene–Late Pliocene (0.73–2.48 m.y.)	87	0.091 ± 0.025	$21.4 \pm 5.1°$	$10.6 \pm 3.6°$
Pliocene (2.48–5.0 m.y.)	27	0.077 ± 0.024	$20.5 \pm 5.8°$[a]	$8.7 \pm 2.7°$

n = number of cones, H_{co}/W_{co} = cone height/cone width ratio, and each parameter is listed with one standard deviation ($\pm 1\ \sigma$).
[a] Failed Mann–Whitney U test with early Pleistocene–late Pliocene.

reach their mature forms. For example, McGetchin et al. (1974) describe four stages in the growth of a scoria cone. By using Northeast Crater (Mount Etna, Sicily) and Parícutin (Mexico) as examples, they report that a scoria cone reaches a fully-developed morphology at a height of approximately 50–60 m. This is when the external talus slope dictates the overall coneform, having buried the earlier, low-rimmed mantle-bedded pyroclastic ring.

The remainder of the 390 cones was dismissed because of an uncertain or exceedingly broad age assignment (as marked on the geologic maps) or a morphometry that was unable to be measured because of an indistinct or buried cone base or some other morphologic peculiarity. Included in the category of 'indistinct cone base' were a few old (Pliocene), highly degraded, low conical hills with relief like an inverted shield.

The five age groups in the San Francisco field provide a temporally-distinct series of cones with which to examine the progressive changes in cone morphology (see Fig. 3). An inspection of the morphometric parameters for the 237 cones in Table 1 reveals a systematic decrease in H_{co}/W_{co} and slope values with an increase in age. Holocene–latest Pleistocene cones have a mean H_{co}/W_{co} value of 0.178, which decreases to a mean H_{co}/W_{co} value of 0.077 for the oldest group of Pliocene cones. For Holocene–latest Pleistocene cones the mean maximum slope angle is 29.7° and the mean average slope angle is 26.4°. For the older Pliocene cone group, the mean maximum slope angle decreases to 20.5° and the mean average slope angle decreases to 8.7°. The detailed morphometry for the San Francisco and Springerville cones is listed in Hooper (1994). A similar pattern of erosional modification has been observed by other authors in different volcanic fields (Scott and Trask, 1971; Bloomfield, 1975; Wood, 1980b; Luhr and Carmichael, 1981; Dohrenwend et al., 1986).

Morphometric analysis also reveals a slight decrease with increasing age in the standard deviation or variability of the H_{co}/W_{co} ratio and the average slope angle (Table 1). This leads to a geomorphologically interesting inference that cone form becomes more uniform with increasing age. Conversely, the variability of the maximum slope angle increases with increasing age, suggesting that many cones are able to retain at least one steep-sloped flank during the life span of the cone. This trend is most likely a

Table 2
Major morphometric parameters for cone age groups in the Springerville volcanic field, AZ

Cone age group	n	Mean H_{co}/W_{co} ($\pm 1\ \sigma$)	Mean maximum slope angle ($\pm 1\ \sigma$)	Mean average slope angle ($\pm 1\ \sigma$)
Middle Pleistocene (0.3–0.97 m.y.)	41	0.127 ± 0.021	$24.7 \pm 3.6°$	$15.6 \pm 3.5°$
Early Pleistocene (0.97–1.67 m.y.)	92	0.109 ± 0.026	$22.3 \pm 4.3°$	$13.0 \pm 3.8°$
Late Pliocene (1.67–1.87 m.y.)	19	0.080 ± 0.026	$18.3 \pm 5.2°$	$9.3 \pm 3.0°$

n = number of cones, H_{co}/W_{co} = cone height/cone width ratio, and each parameter is listed with one standard deviation ($\pm 1\ \sigma$).

manifestation of an initial coneform that was not perfectly symmetrical or contained a heterogeneous internal unit (e.g., resistant agglutinate).

The San Francisco volcanic field is bordered on the south and southwest by a group of Miocene–early Pliocene volcanic rocks informally referred to as 'rim basalts' (e.g., Wood, 1980b; Tanaka et al., 1986, 1990) because they occur along the Mogollon Rim, the physiographic feature that defines the southern margin of the Colorado Plateau. Potassium–Argon ages suggest rim basalt volcanism is primarily Miocene in age and occurred during the period from 5 to 8 m.y. (Luedke and Smith, 1978; Reynolds, 1988; Tanaka et al., 1990). As an ancillary data set to study highly degraded scoria cones older than 5 m.y., we will briefly discuss a group of 25 cones along the loosely defined southwest margin of the San Francisco field westward to the vicinity of the town of Ash Fork (see Fig. 3). This group of mostly Miocene-age cones has a mean H_{co}/W_{co} ratio of 0.058 ± 0.024, a mean maximum slope angle of $15.1 \pm 6.2°$, and a mean average slope angle of $6.6 \pm 2.7°$ (Hooper, 1994). Supporting low H_{co}/W_{co} values and diminished slope angles, these cones display the anticipated trend of increasing erosional modification with increasing age. The lava flows and scoria cones of rim basalt age may be genetically distinct from the highly varied lavas of the San Francisco volcanic field, but we make the assumption that they form a continuous geomorphologic sequence and offer a continuation of the degradational pattern seen in the younger cones of the San Francisco field.

Geologic maps by Condit (1991, 1995), and Condit et al. (in press) divide the volcanic rocks of the Springerville field into five categories, three of which contain an adequate number of scoria cones for statistical analysis. From youngest to oldest, the three cone age groups defined from the available geologic maps are: middle Pleistocene (0.3 to 0.97 m.y.), early Pleistocene (0.97 to 1.67 m.y.), and late Pliocene (1.67 to 1.87 m.y.). Using the same procedures and criteria as in the San Francisco field, complete morphometric parameters were calculated for 152 of the approximately 205 scoria cones in the Springerville volcanic field (Table 2 and Fig. 4). Excluded from the analysis in Table 2 were 27 cones with only measurements of maximum cone slope

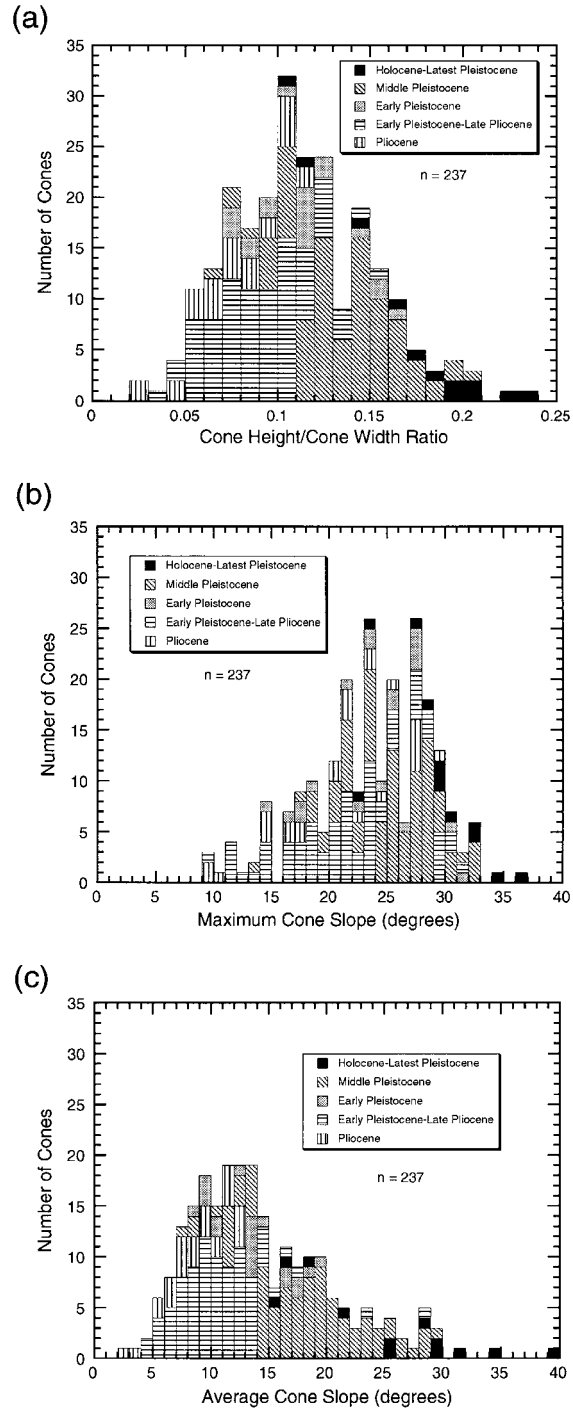

Fig. 5. Histograms for each of the major morphometric parameters for scoria cones in the San Francisco volcanic field. Total number of cones is 237. (a) Cone height/cone width ratio (H_{co}/W_{co}). (b) Maximum cone slope angle. (c) Average cone slope angle.

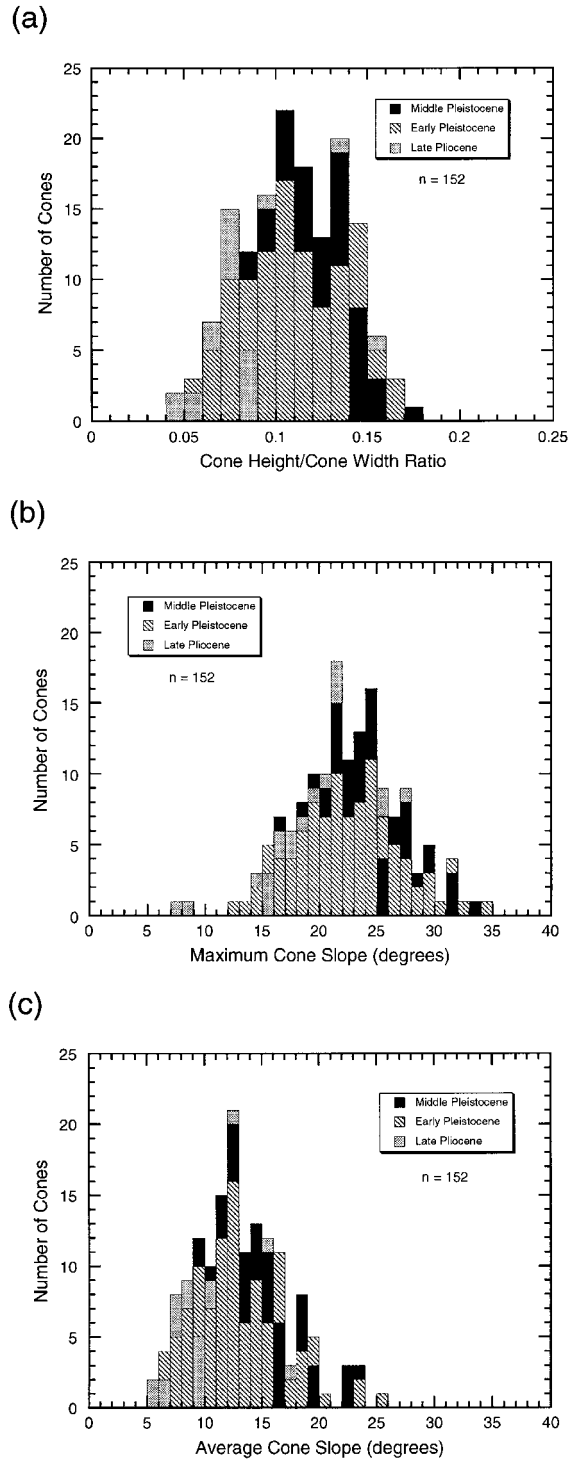

Fig. 6. Histograms for each of the major morphometric parameters for scoria cones in the Springerville volcanic field. Total number of cones is 152. (a) Cone height/cone width ratio (H_{co}/W_{co}). (b) Maximum cone slope angle. (c) Average cone slope angle.

angle. Variations in cone morphometry with time repeat the same trends that were found in the San Francisco field.

Figs. 5 and 6 display the relative frequency distribution for each of the morphometric parameters. Because these parameters have relatively large standard deviations (Tables 1 and 2), Mann–Whitney U tests were performed to compare the distribution between cone age groups. Using a significance level of $\alpha = 0.05$, the statistical tests were conducted for each age group in both volcanic fields. Each of the H_{co}/W_{co}, maximum slope angle, and average slope angle parameters were checked. Of all these statistical analyses, only the maximum slope evaluation between early Pleistocene–late Pliocene and Pliocene cones in the San Francisco volcanic field resulted in a test that showed no difference between the population distribution of the age groups. Therefore, we will treat each cone age group as a distinct population.

The ratio of crater depth to crater width (D_{cr}/W_{cr}) was observed to decrease with time. Applying examples from both volcanic fields, 14 scoria cones with craters were used in a cursory examination of this trend. The criteria for selection were that each cone had to have a radiometric age (or similar chronostratigraphic data) with a narrow range of error and that each cone had an unbreached crater. This strict combination eliminated many potential examples. After plotting an exponential fit (as well as a linear fit) to the selected population, we can infer that the average scoria cone in these two Arizona volcanic fields will lose its crater to erosion after approximately 1.25 m.y. (Fig. 7).

The general, long-term morphologic changes experienced by a scoria cone in the semi-arid study sites of Arizona can be summarized. After the conclusion of eruptive activity, the typical scoria cone will have a conical to slightly elongated shape (Fig. 8). The summit crater is often bowl-shaped, but can also be elongated or elliptical. Some cones are breached during construction, causing uneven crater

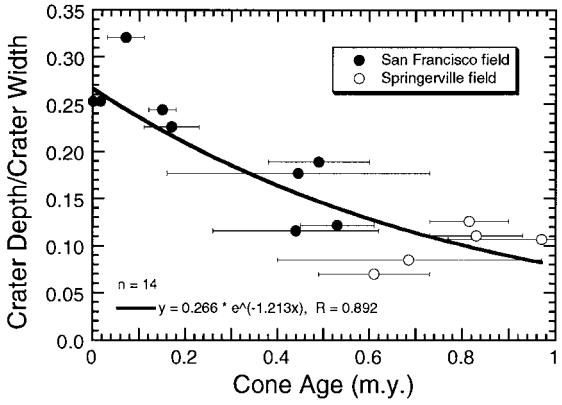

Fig. 7. Fourteen scoria cones from both volcanic fields were used to plot the decrease in the ratio of crater depth to crater width (D_{cr} / W_{cr}) with time. Error bars for the age determinations and the exponential fit are shown.

rim heights or other irregularities. Downslope transport of the pyroclastic material is accomplished by a variety of processes, such as overland flow and rainsplash (Hooper, 1994; unpub. data). Rill and debris flow processes may also contribute to the erosional modification of these landforms (Dohrenwend et al., 1986; Renault, 1989). The transport of material to the cone periphery will increase the debris-apron volume and enlarge the basal diameter of the cone. Changes are also seen within the crater as crater depth decreases by slumping, debris flows, and the general downslope transport of material that was previously a constituent of the crater rim or crater wall. Such degradational changes have been observed by Inbar et al. (1994), who report 10 m of infilling since 1957 in the Parícutin crater, Mexico. While a crater is being partially infilled by erosional processes, a gully may breach a progressively lowering crater rim, thus producing a second type of breach. Cone height progressively decreases to the point that the crater will be completely removed by erosion and the cone may now resemble a cinder dome or mound. The eventual obscuration and removal of the crater due to erosion signifies the loss of a distinguishing characteristic of these volcanic landforms. In a simple classification, youthful cones possess a crater while older cones have lost the crater to erosion. Further erosion reduces the cone to

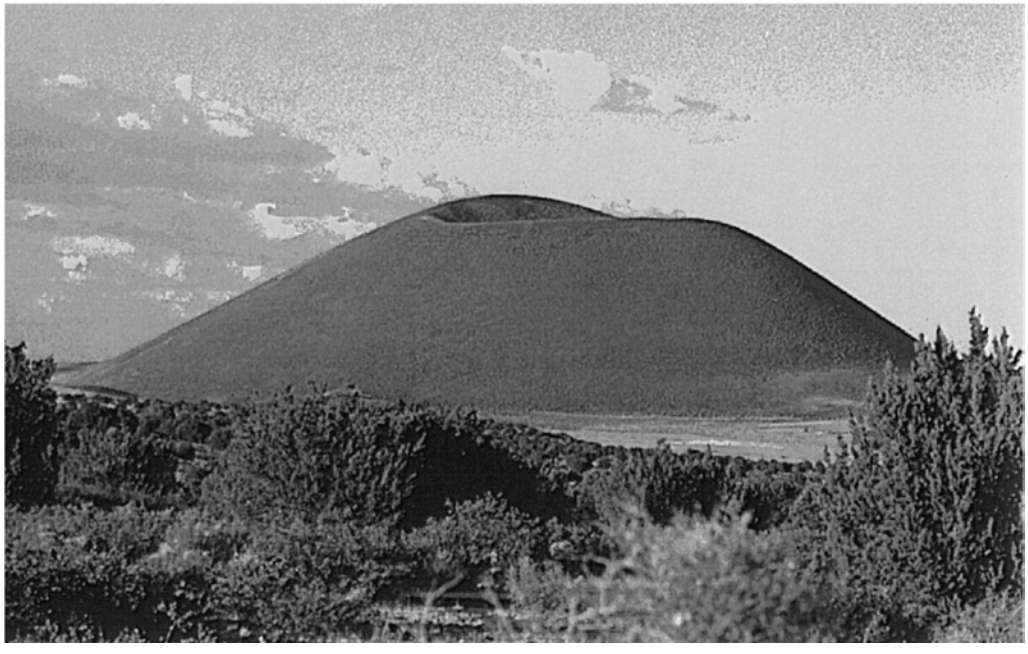

Fig. 8. Merriam Crater (V3036) in the San Francisco volcanic field has the typical morphology of a youthful, late Pleistocene cone. It is 370 m high with steep slopes, radial symmetry, and a sharp-rimmed crater (partially visible in the photograph taken with a view to the northeast). Merriam Crater has been dated at 0.15 ± 0.03 m.y. (see Tanaka et al., 1990).

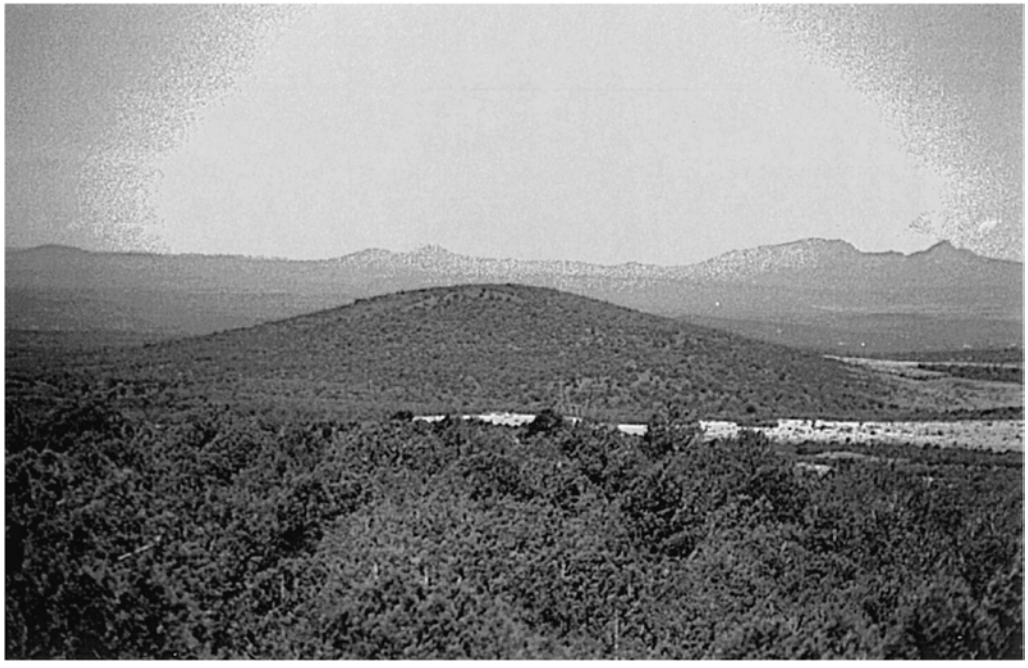

Fig. 9. Photograph of an unnamed cone (V2133) near Ash Fork, AZ, along the margin of the San Francisco volcanic field (see Fig. 3 and text). It has been mapped as part of a Miocene–early Pliocene group of volcanic rocks (Luedke and Smith, 1978) and demonstrates the typical profile of an 'old', degraded scoria cone that has lost its crater to erosional processes. The cone is 67 m high and was photographed looking northwest.

a low-relief or shield-like hill with minimal slope angles (Fig. 9). These degraded cones are often overlooked as researchers concentrate on the more youthful volcanoes.

Additionally, gullies are present on many of the cones in each study site. The youngest cones do not have gullies because the infiltration capacity is too high and runoff is unable to be generated. Incipient gully formation is characterized by unevenly spaced rills and gullies, usually occurring along the lower cone slopes near the base. On older cones they increase in width and depth until culminating in large, widely-spaced gullies or ravines.

6. Diffusion-equation model

The analytical models of Culling (1960, 1963, 1965) represented the first attempt to develop a mathematical theory of slope erosion with a general diffusion-like equation similar to that derived by Fourier (1878) for the conduction of heat in solids, or by Fick (1855) for chemical dispersion. More recently, several workers have applied a diffusion-equation model to two-dimensional profiles to estimate the age of fault scarps and marine, lacustrine, or fluvial terrace scarps (e.g., Nash, 1980a,b, 1984; Colman and Watson, 1983; Hanks et al., 1984; Mayer, 1984; Andrews and Hanks, 1985; Pierce and Colman, 1986; Andrews and Bucknam, 1987). Bursik (1991) used a similarity solution to a generalized diffusion equation to estimate the relative ages of glacial moraines in the Sierra Nevada, CA.

Fundamental assumptions of a diffusion-equation model include local conservation of mass and downslope transport proceeding at a rate proportional to a power of the slope and slope length. In one spatial dimension, this can be expressed as:

$$M = Dx^m\left(\frac{\partial z}{\partial x}\right)n \qquad (2)$$

where M is the rate of downslope transport or mass flux, D is a constant of proportionality (where the transport rate coefficient and density have been com-

bined to produce the diffusion coefficient) that is assumed not to vary with position or time, x is a horizontal distance, $\partial z/\partial x$ is the topographic gradient for a profile orthogonal to the hillslope. The exponential parameters m and n are a function of the erosional process and are discussed below.

Sediment transport processes on slopes are either linearly diffusive if downslope movement is directly proportional to the surface gradient to the first power, or nonlinearly diffusive if downslope movement is more dependent upon slope length and not proportional simply to the local slope raised to the first power. Linear diffusive agents of erosion include rainsplash (raindrop impact), soil creep, freeze–thaw movements, and bioturbation (e.g., Culling, 1960, 1963, 1965; Kirkby, 1971; Carson and Kirkby, 1972; Pierce and Colman, 1986; Colman, 1987). For these processes the downslope movement is directly proportional to surface gradient to the first power and $m = 0$ and $n = 1$.

Dynamic simulation models that treat the transport of material must consider the conservation of mass. Such continuity relations have been applied to hillslopes (Kirkby, 1971) and require that an increase or decrease in the downslope flow rate of material over a straight line segment of the hillslope will cause the elevation of the segment to decrease or increase with time. Using the simpler form for one spatial dimension, this relationship can be expressed as:

$$\frac{\partial z}{\partial t} = \frac{\partial M}{\partial x} \tag{3}$$

where t is time and the other terms have previously been defined.

Finally, combining Eqs. (2) and (3) yields the linear diffusion equation, which can be written to describe a three-dimensional landform:

$$\frac{\partial z}{\partial t} = D_x \frac{\partial^2 z}{\partial x^2} + D_y \frac{\partial^2 z}{\partial y^2} \tag{4}$$

where x is the first horizontal coordinate direction, y is the second horizontal coordinate direction, z is the vertical coordinate direction or elevation, D_x is the diffusion coefficient in the x-direction, and D_y is the diffusion coefficient in the y-direction. This equation assumes the rate of diffusive flow varies according to direction (i.e., it is anisotropic) and can easily be simplified for isotropic diffusion. Rigorous mathematical methods of solution and a discussion of initial and boundary conditions can be found in the standard works of Carslaw and Jaeger (1959) and Crank (1975).

A second category of transport processes to be modeled follows a nonlinear transport law. These include slope wash (soil wash or sheet wash) both with and without gullying. Because these transport processes are slope-length dependent, they are more complex to describe mathematically, yielding approximately $m = 0.3–1.0$ and $n = 1.3–2$ for slope wash without gullying; and $m = 1–2$ and $n = 1.3–2$ for slope wash with gullying (e.g., Kirkby, 1971; Carson and Kirkby, 1972; Pierce and Colman, 1986; Colman, 1987). To deal with the nonlinear behavior of these processes, but in the context that linear diffusion is still to be the first-order approximation, a generalization of Eq. (4) can be written as:

$$\frac{\partial z}{\partial t} = \frac{\partial}{\partial x}\left[F\left(x, \frac{\partial z}{\partial x}\right)\right] + \frac{\partial}{\partial y}\left[F\left(y, \frac{\partial z}{\partial y}\right)\right] \tag{5}$$

where the function F is arbitrary, making downslope transport or mass flux a nonlinear function of slope. The diffusion coefficient is incorporated in function F.

For computer applications and a numerical solution, the diffusion equation was translated to a three-dimensional, explicit finite-difference scheme utilizing a grid of unit cells, each with a topographic elevation (z-direction) and extending in the x- and y-directions. Taylor series expansion can be used to convert the diffusion equation to a finite-difference form (e.g., Richtmyer and Morton, 1967; Harbaugh and Bonham-Carter, 1970; Crank, 1975). Finite-difference analysis simulates the movement of material into (aggradation) or out of (erosion) the cell being evaluated in a manner proportional to the elevation difference between neighboring cells (i.e., slope) and the erodibility (i.e., diffusion coefficient) between cells. Mass flux is checked so that it cannot exceed the amount of available sediment.

7. Computer simulation

Our approach to computer simulation is to begin with a simplified model and then enhance the model as physical parameters and processes become better understood. The various erosional processes occur at different frequencies, rates, and seasons. A diffusion-equation model is an approximation of these complex processes. For this study, computer simulation by a numerical model treats the internal structure of a scoria cone—loose pyroclastic layers occasionally interbedded with agglutinated layers or lava flows—as a homogeneous unit that does not produce a significant variation in erosion rate when observed over a period of tens to hundreds of thousands of years. We assume that each cone is monogenetic (e.g., Macdonald, 1972; Bloomfield, 1975; Williams and McBirney, 1979; Wood, 1979) rather than polycyclic or episodic (e.g., Turrin and Renne, 1987; Crowe et al., 1988, 1989; Renault et al., 1988; Renault, 1989; Wells et al., 1990, 1992). Furthermore, we must make certain assumptions regarding lithology and composition. Using data supplied by Settle (1979), Wood (1980a) compiled the morphometric relationships for 910 cones of various ages from several volcanic regions. He concluded that the ratios for cone height/width (H_{co}/W_{co}) and crater width/cone width (W_{cr}/W_{co}) apparently remain consistent for cones in diverse tectonic settings, and that these morphometric relationships appear to be valid for a wide range of particle size and chemistry. He further stated that cone slopes (angle of repose) are not strongly dependent on the particle size distribution of constituent fragments. For the model presented in this study, we concur with the conclusions of Wood (1980a). Finally, for the simulations presented in this report, we have used the simplest geometry for these conical landforms. The model cone is symmetrical rather than slightly elongated or even breached.

Table 3
Parameters and initial values for the finite-difference grid and modeled scoria cone

Cell size	4×4 m
Grid or matrix size	400×400 cells
Cone height (H_{co})	170 m
Cone width or basal diameter (W_{co})	876 m
Cone height/width ratio (H_{co} / W_{co})	0.194
Crater width or crater diameter (W_{cr})	292 m
Crater depth (D_{cr})	67 m
Crater width/cone width ratio (W_{cr} / W_{co})	0.333
Crater depth/crater width (D_{cr} / W_{cr})	0.229
Initial maximum and average cone slope	30.2°
Volume	50.0×10^6 m^3

The simulation of cone erosion employed a cell size of 4×4 m and operated upon a 400×400 (1600×1600 m) grid or matrix of elevation values from a digitized scoria cone with a fully-developed, youthful, and idealized morphology. The initial morphology of the model or test cone used in the simulations approximated a right circular cone truncated at the top by a smaller inverted cone to simulate the summit crater. Geometry of the model cone was determined by measuring from topographic maps the morphometry of 70 unbreached, Holocene to latest Pleistocene cones from several volcanic fields in a variety of locations, including Hawaii, western USA, Mt. Etna (Sicily), Kamchatka (Russia), and the Trans-Mexican volcanic belt. The morphometric parameters of these cones are listed in Hooper (1994, 1995). The objective of this selection was to obtain the idealized morphology of a conical, unbreached scoria cone. Geometric relations and the arithmetic means were then used to construct the model cone that was used in the simulations (Table 3).

Computer simulation was stopped after 300,000 time steps. A time step or time increment is one pass through the computer algorithm evaluating the grid of digital topography. Because the selected finite-difference scheme can produce an unstable solution, the

Fig. 10. (a–h). Profiles taken at appropriate time intervals during computer-simulated erosion record the changing morphology of the model scoria cone. These profiles pass through the center of the model cone and are displayed without vertical exaggeration. Degradation progresses from the initial conical form (time step 0), through rounding of the crater rim and crater degradation, through a stage with a mound or shield-like hill, and finally into a nearly flat landform (time step 300,000). The crater has been completely removed by erosion by time step 6500 for the nonlinear model and by time step 15,500 for the linear model. A time step (or time increment) is one pass through the computer algorithm evaluating the grid of unit cells.

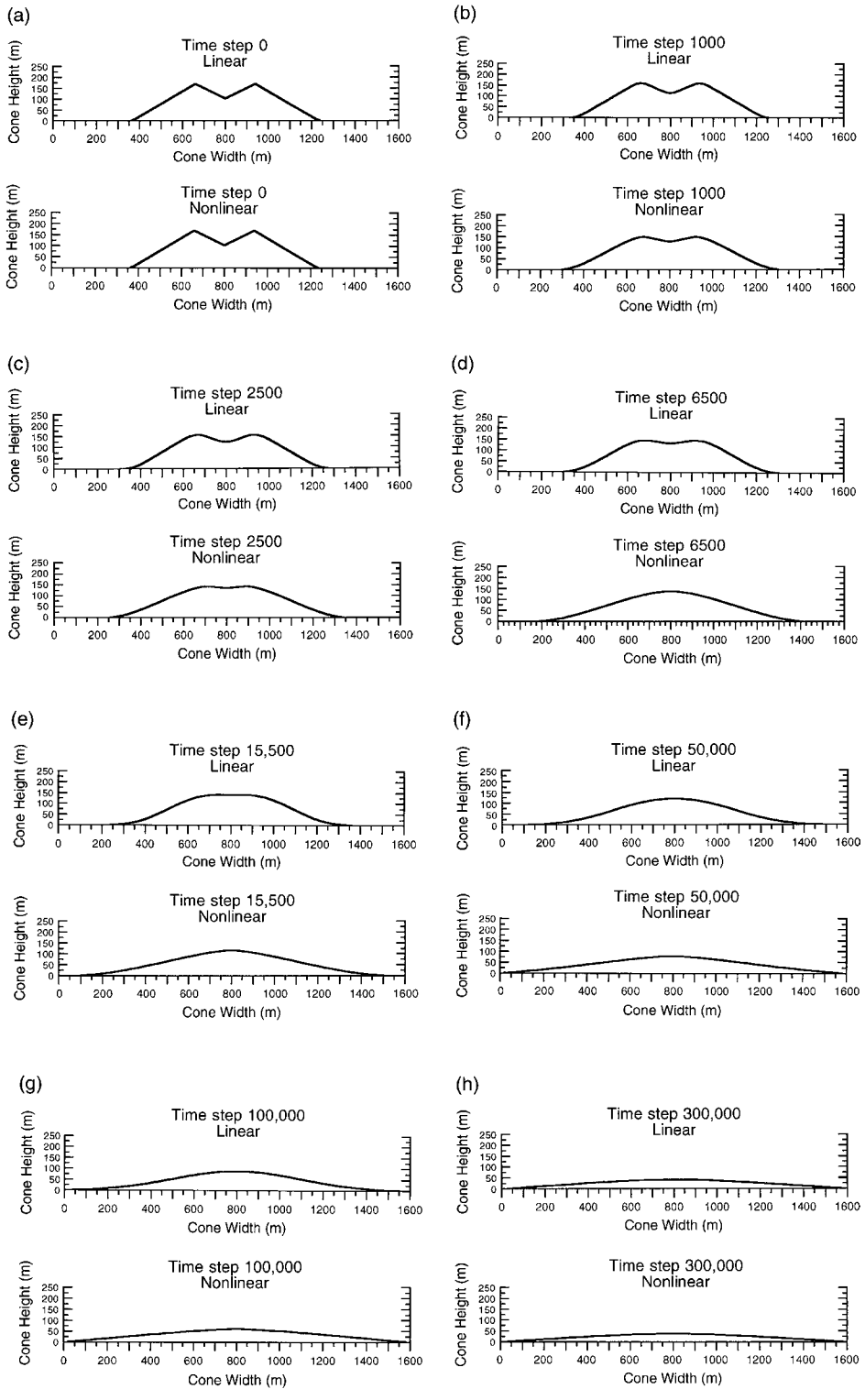
(a)
Time step 0
Linear
Time step 0
Nonlinear
(b)
Time step 1000
Linear
Time step 1000
Nonlinear
(c)
Time step 2500
Linear
Time step 2500
Nonlinear
(d)
Time step 6500
Linear
Time step 6500
Nonlinear
(e)
Time step 15,500
Linear
Time step 15,500
Nonlinear
(f)
Time step 50,000
Linear
Time step 50,000
Nonlinear
(g)
Time step 100,000
Linear
Time step 100,000
Nonlinear
(h)
Time step 300,000
Linear
Time step 300,000
Nonlinear
Cone Height (m)
Cone Width (m)
0 50 100 150 200 250
0 200 400 600 800 1000 1200 1400 1600

time step and diffusion coefficient must be kept sufficiently small to prevent amplification of errors or oscillations in the solution (e.g., Crank, 1975). Each simulation was conducted with a model diffusion coefficient of $D_m = 1.0$ m^2/time step for the linear model and $D_m = 1.0$ m/time step for the nonlinear version of the erosion model. Regarding units, in a linear model the diffusion term has dimensions [length^2/time] and is often expressed in a geomorphologic study in units of square meters per thousand years [m^2/kyr]. For the nonlinear derivation, the diffusion term has dimensions [length/time] and has units of meters per thousand years [m/kyr]. Marking the final assignment of all parameters, simulations employing the linear (creep and rainsplash) model used values of $m = 0$ and $n = 1$ in Eq. (2), while the nonlinear (slope wash with gullying) model operated with values of $m = 2$ and $n = 2$.

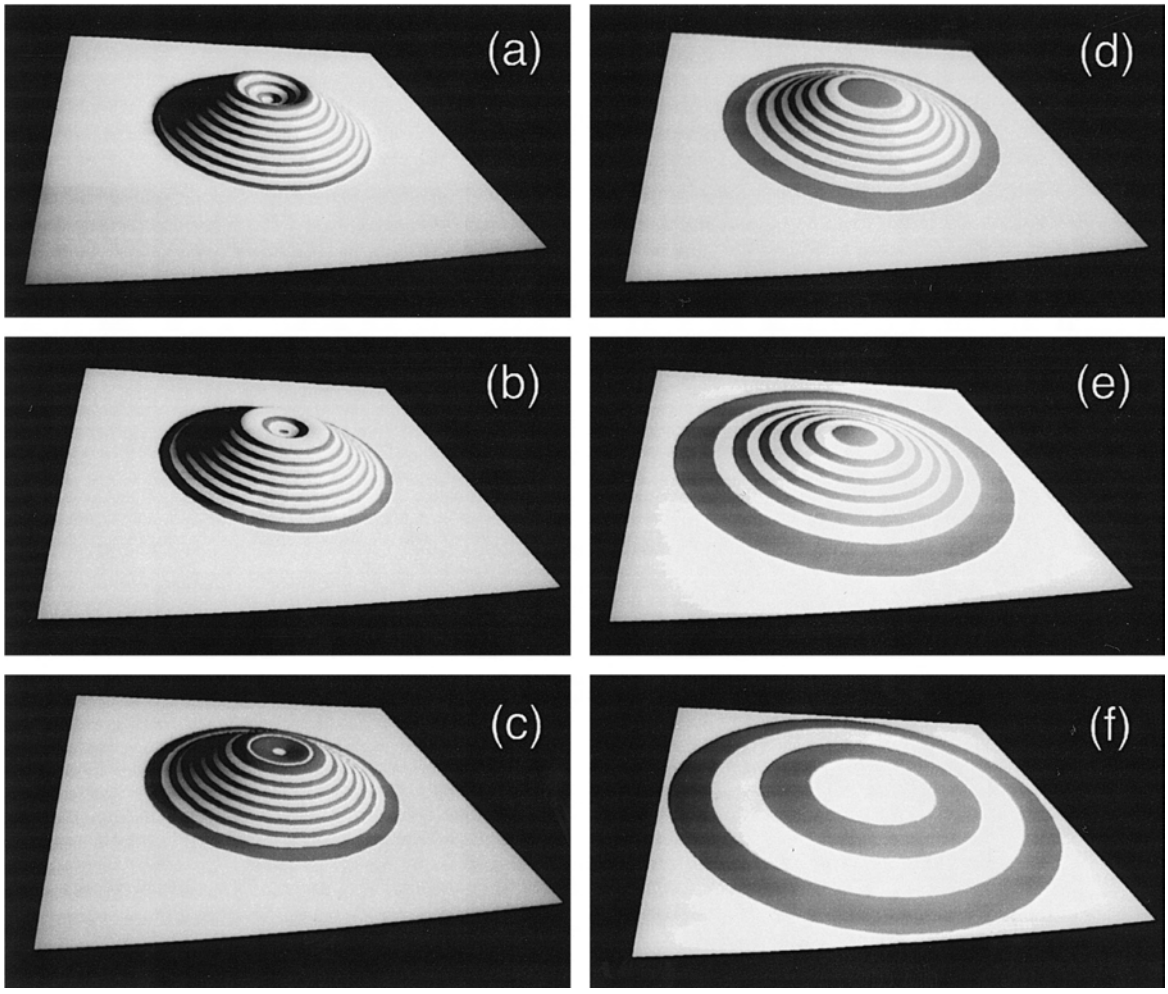

Fig. 11. A series of photographs was assembled to display the results from the application of the linear diffusion-equation model. Three-dimensional perspectives or views exhibit different degradational stages in the erosion of the model cone. Using the visualization algorithm by Kover (1995), each image is a shaded digital terrain model (DTM) and was constructed by connecting data triplets (x, y, z) to form a network of triangles (TIN or triangulated irregular network). Each color band represents a thickness of approximately 11.3 m. The stages of simulated erosion are: (a) time step 0, (b) time step 2500, (c) time step 6500, (d) time step 15,500, (e) time step 50,000, and (f) time step 300,000.

Progressive degradation was observed from the initial conical form (time step 0), through rounding of the crater rim and crater degradation, through a stage with a mound or shield-like hill, and finally into a severely degraded, low-relief landform with a low H_{co}/W_{co} ratio. These morphologic changes are demonstrated by a series of profiles or cross-sections taken through the center of the model cone during simulated erosion (Fig. 10) and by three-dimensional perspectives of critical time steps (Figs. 11 and 12). The characteristic form of the cone flanks in these profiles illustrates a fundamental difference in hillslope processes which can be summarized by stating that the relatively slow mass movement by simulated soil creep and rainsplash processes yields a convex hillslope typical of linear diffusion, whereas relatively more rapid mass movement from simulated overland flow processes such as slope wash yields a concave hillslope typical of nonlinear transport laws.

As the three-dimensional views in Fig. 12 illustrate, the nonlinear model does not show individual gullies as in cellular automata models (e.g., Chase, 1992; Murray and Paola, 1994). For long-term elevation changes it is necessary to model the average

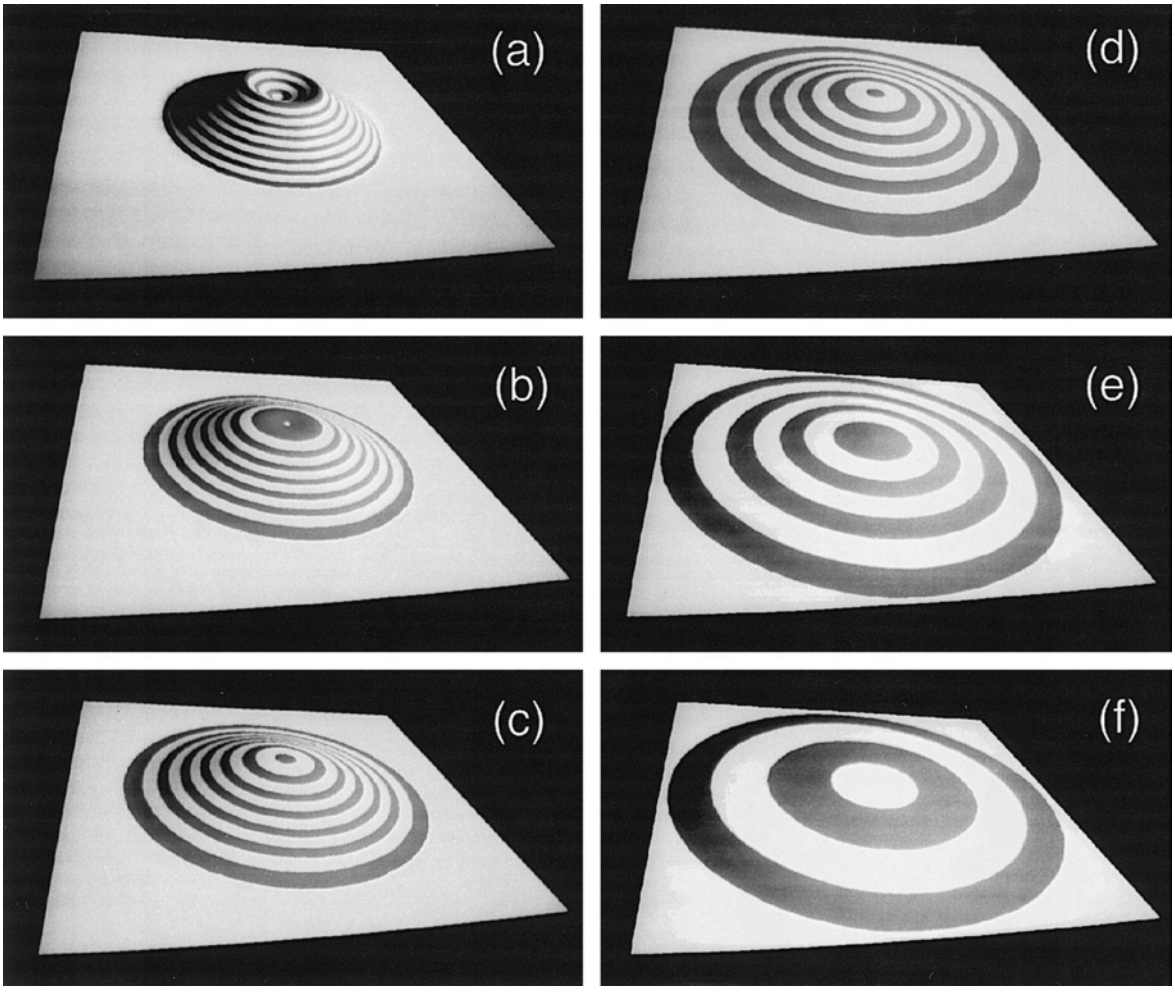

Fig. 12. This series of photographs displays the results of the nonlinear (slope wash with gullying) transport model. Each color band represents a thickness of approximately 11.3 m. The stages of simulated erosion are: (a) time step 0, (b) time step 2500, (c) time step 6500, (d) time step 15,500, (e) time step 50,000, and (f) time step 300,000.

effect of the degradational processes with time. Therefore, the aggregate effect of all processes or events is modeled and each time step represents how the cone is expected to look, on average, at any given time. This causes our model cone to appear smoother than its field equivalent.

The difference in erosion rate between the two transport laws is further demonstrated by recording when the point of greatest elevation on the cone shifts from the crater rim to a point in the center of the cone following the obscuration or complete removal of the crater by erosion. This transition in maximum elevation occurs approximately at time step 6500 for the nonlinear model and time step 15,500 for the linear model (see Figs. 10–12).

Additional results from the computer simulations are displayed in Fig. 13, which depicts the reduction in H_{co}/W_{co}, maximum slope angle, and average slope angle with increasing age (measured in time steps) for both versions of the numerical model. Maximum cone slope angle was calculated over a five-cell (or 20-m) interval. This spacing was selected to approximate the horizontal distance used in measuring the maximum slope angle from topographic maps, yet not sacrificing the greater detail provided by the grid network in the simulations. The

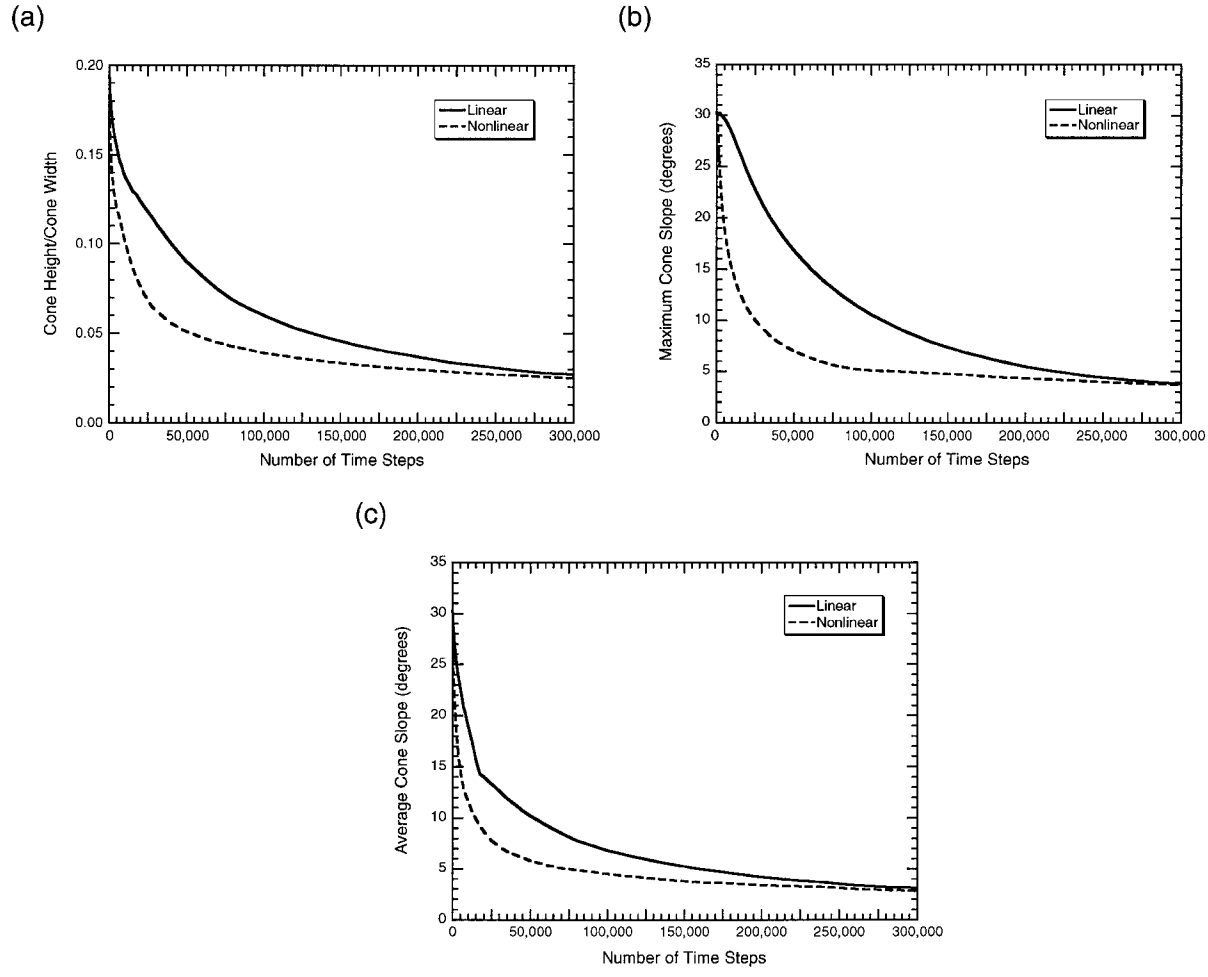

Fig. 13. Plots depicting the decrease in the major morphometric parameters with increasing age (measured in time steps) for computer-simulated erosion of the modeled scoria cone by two different transport laws. (a) Cone height/cone width ratio (H_{co}/W_{co}). (b) Maximum cone slope angle. (c) Average cone slope angle. The nickpoint around time step 15,500 (linear model) is related to crater degradation.

initial maximum slope angle for the model cone is 30.2°, but this slope is only maintained for the first 300 time steps by the nonlinear model, while the linear model preserves this maximum slope angle for 2150 time steps.

We can begin to demonstrate how our numerical model can be modified to treat the naturally occurring variations found in scoria cone morphology. For example, some cones have a crater rim or a portion of a crater rim capped by more resistant agglutinated layers forming a lava ruff or collar. To simulate this condition, the algorithm was modified such that half the crater rim was assigned a lower erosion rate by reducing the diffusion coefficient, D_m. The width or height of this resistant rim can be varied as well. Several different combinations were selected and run through the erosion model. As anticipated, these runs produced a cone with uneven crater rims. Being slower to erode, the rim with the resistant cap was initially higher in elevation and generally more angular in appearance. After the more resistant layer was removed, this half of the cone, including flanks and debris apron, proceeded with degradation in a manner similar in appearance and symmetry to the unaffected half. Fig. 14 features two simulation runs, one with the linear and the other with the nonlinear versions of the numerical model. For each of these the resistant layer was set at 5 m thick and extended downward from the top of the crater rim (the initial morphology was not altered). For the resistant layer only, the diffusion coefficient in the linear model was reduced to $D_m = 0.01$ m^2/time step ($D_m = 0.01$ m/time step in the nonlinear version) rather than the usual value of $D_m = 1.0$ m^2/time step ($D_m = 1.0$ m/time step in the nonlinear version), which was used elsewhere around the model cone and became the sole value after removal of the resistant cap. The resistant half of the crater rim appears on the right-hand side of the cone in the figures. An additional discussion on how the simulation algorithm can be

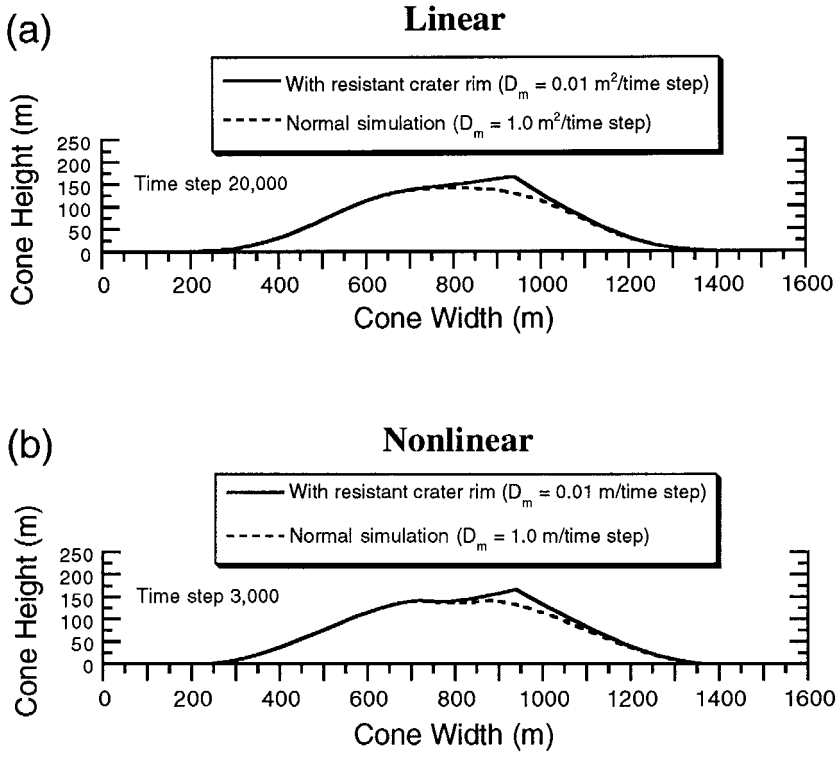

Fig. 14. Simulation runs using a more resistant (lower diffusion coefficient, D_m) for the uppermost 5 m at the top of the right half of the crater rim. (a) The difference in erosional profiles at time step 20,000 with the linear diffusion-equation model. (b) The difference in erosional profiles at time step 3000 with the nonlinear model. See text for further explanation.

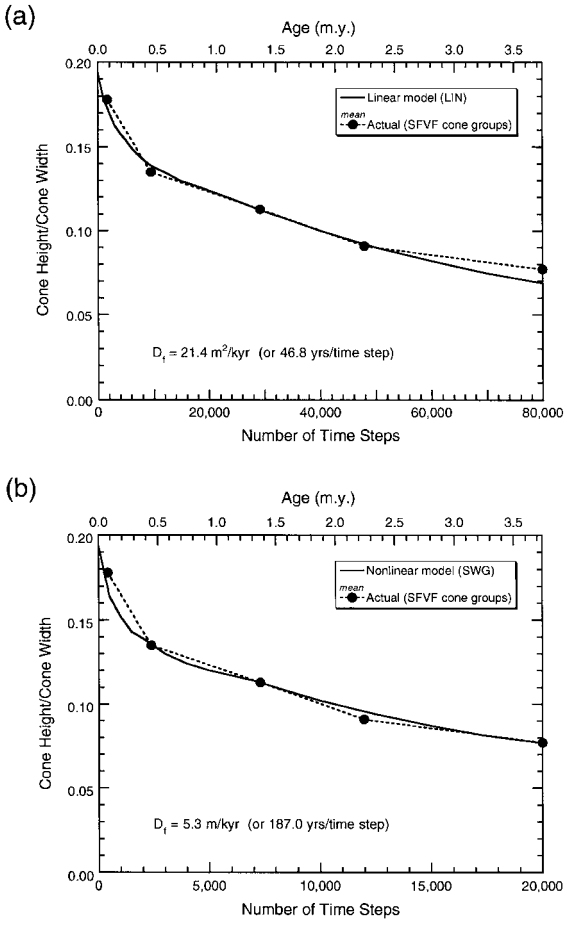

Fig. 15. Figures demonstrating the correlation of actual cone degradation with model cone degradation. Mean H_{co}/W_{co} values for the five cone age groups in the San Francisco volcanic field are plotted versus the mean of their respective age groups (confidence limits omitted for clarity). Superimposed upon these data are the calibrated curves from the (a) linear diffusion-equation model (LIN) with $D_m = 1.0$ m^2/time step and (b) nonlinear model (simulating slope wash with gullying or SWG) with $D_m =$ 1.0 m/time step.

revised to treat secondary or external modifications and on the omissions of the model can be found in Hooper (1994, 1995).

8. Comparison of model and field results

One method by which to compare field and model data is to match the mean H_{co}/W_{co} values for each cone age group with the H_{co}/W_{co} values from computer simulations. This procedure yields a correlation of results and requires an inverse-solution approach to determine the diffusion coefficient for cone erosion in each volcanic field. The erosion rate in each

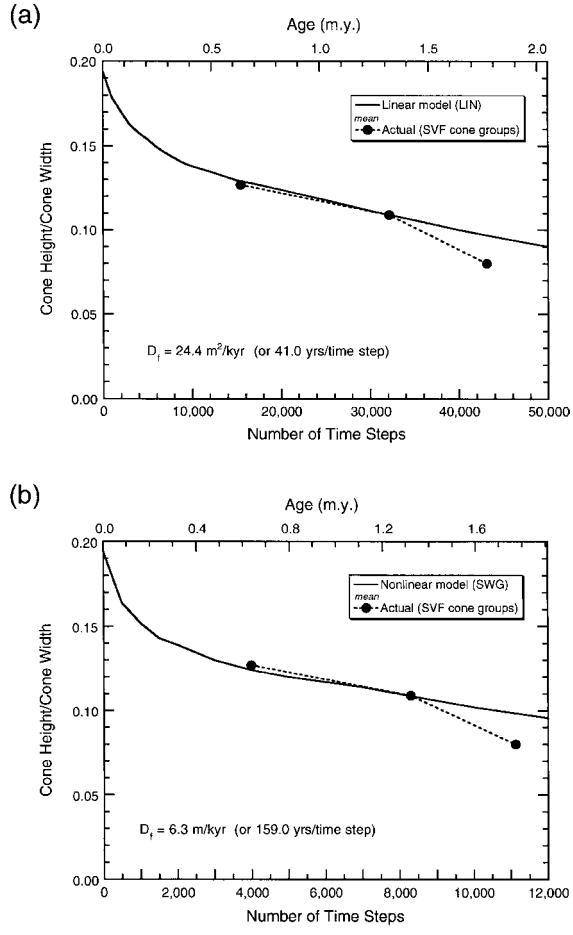

Fig. 16. Figures demonstrating the correlation of actual cone degradation with model cone degradation. Mean H_{co}/W_{co} values for the three cone age groups in the Springerville volcanic field are plotted versus the mean of their respective age groups (confidence limits omitted for clarity). Superimposed upon these data are the calibrated curves from the (a) linear diffusion-equation model (LIN) with $D_m = 1.0$ m^2/time step and (b) nonlinear model (simulating slope wash with gullying or SWG) with $D_m =$ 1.0 m/time step. The late Pliocene cone group plots below the anticipated values derived from the simulation. This may indicate a period of increased erosion.

Table 4
Comparison of calculated diffusion coefficient (D_f) values for several basaltic volcanic fields

Volcanic field/location	Linear model D_f (m^2/kyr)	Nonlinear model D_f (m/kyr)	Climate	Mean annual precipitation (mm)	Source for precipitation data
Michoacán-Guanajuato (central Mexico)[a]	124.6	22.2	Temperate–tropical	710	Mosiño-Alemán and García, 1974
Springerville (AZ, USA)	24.4	6.3	Semi-arid	480	Sellers and Hill, 1974
San Francisco (AZ, USA)	21.4[c]	5.3	Semi-arid	435	Sellers and Hill, 1974
Cima (CA, USA)[b]	8.2	1.5	Arid	110	Ruffner, 1985

[a] Data for the Michoacán-Guanajuato volcanic field from Hooper (1994, 1995).
[b] Data for the Cima volcanic field from Hooper (1994).
[c] This value was reported as 24.1 m^2/kyr in Hooper (1995), but it has since been recalculated after placing the Pleistocene–Pliocene boundary back at 2 m.y., as was used by the original workers (Wolfe, pers. comm., 1995) when compiling their correlation diagrams for the geologic maps of the San Francisco volcanic field. This boundary has most recently been placed at 1.64 m.y. (e.g., Aguirre and Pasini, 1985) and a brief note on this topic is included in the geologic maps (Moore and Wolfe, 1987; Newhall et al., 1987; Ulrich and Bailey, 1987; Wolfe et al., 1987a,b). For the nonlinear model, this correction actually improved the fit between model and actual cone groups and the D_f value was not changed.

Table 5
Diffusion coefficient (D_f) values for various geomorphologic and environmental settings

Location and geologic structure	D_f (m^2/kyr)	Source
Lake Algonquin wave-cut bluffs, MI (USA)	12	Nash, 1980a
Nipissing Great Lakes, wave-cut bluffs, MI (USA)	12	
Drum Mountains fault scarps, UT (USA)	0.44	Nash, 1980b
Lake Bonneville shoreline scarps, UT (USA)	0.9	Colman and Watson, 1983
Santa Cruz sea cliffs, CA (USA)	11	Hanks et al., 1984
Lake Bonneville shoreline scarps, UT (USA)	1.1	
Raymond fault scarp, CA (USA)	16	
Drum Mountains, Fish Springs Range, Oquirrh Mountains, and Sheeprock Mountains fault scarps, UT (USA)	1.1	
West Yellowstone Basin fluvial terrace scarps, MT (USA)	2.00 ± 0.38	Nash, 1984 (Table 3)
Delta progradation		
Fraser River, British Columbia (Canada)	2.4×10^7	Kenyon and Turcotte, 1985
Rhine River at Lake Constance (Germany–Switzerland–Austria)	3.0×10^7	
Mississippi River (SW Pass), LA (USA)	5.6×10^8	
Hillslope erosion of peridotite sheet, New Caledonia (French overseas territory)	1.8×10^4	Moretti and Turcotte, 1985
Lake Bonneville shoreline scarps, UT (USA)	0.57 to 0.98	Pierce and Colman, 1986 (Table 5)[a]
Drum Mountains fault scarps, UT (USA)	0.57 to 0.98	
Lake Bonneville shoreline scarps, UT (USA)	0.46	Andrews and Bucknam, 1987 (Table 1)[b]
Lake Lahontan shoreline scarps, NV (USA)	0.90	
Olympic Peninsula hollows, WA (USA)	4.2 ± 2.3	Reneau et al., 1989
Lee Vining Canyon, lateral moraines, CA (USA)	4.1, 5.3	M. Bursik (unpublished data)

[a] Normalized to scarp height and orientation.
[b] Linear plus cubic transport law.

volcanic field can be determined by solving for D_f in the simple yet powerful relationship:

$$D_f t_f = D_m t_m \quad (6)$$

where D_f is the diffusion coefficient for a cone age group or a similar collection of cones in the volcanic field, t_f is the mean age for the cone age group or cones in the volcanic field, D_m is the diffusion coefficient used in the computer simulation model, and t_m is the model age as measured in computer time steps or increments. The values for t_m were found when the H_{co}/W_{co} values from computer simulations matched the mean H_{co}/W_{co} values for each cone age group. Once this relationship has been solved, the length of a computer time step can easily be calculated as years per time step.

This correlation between changing H_{co}/W_{co} value, cone age, and computer time step can be expressed graphically and was used to derive comprehensive values of D_f for each of the volcanic fields (Figs. 15 and 16). For the San Francisco field, D_f had a calculated value of 21.4 m^2/kyr for the linear model and 5.3 m/kyr for the nonlinear model, while for the Springerville field D_f had a calculated value of 24.4 m^2/kyr for the linear model and 6.3 m/kyr for the nonlinear model. These measures of the degradation rate of basaltic scoria cones in a volcanic field can be compared to other volcanic fields for which they were obtained by the same procedure (Table 4). An increase in the D_f value indicates an increase in the effective erosion rate. Since precipitation rates increase with an increase in elevation in this region, the higher average elevation for the Springerville field is probably the reason why this field has a slightly higher erosion rate than the San Francisco field.

The degradation of a variety of landforms has been examined with a diffusion-equation approach. While some authors refer to the D_f parameter as the transport coefficient, our results are similar to these other studies (Table 5). Since most of the other studies utilized a simpler, one-dimensional linear-diffusion model, these differences may be attributed to variations in climate, age or type of landform, model type, and lithology or nature of slope material.

Normalized profiles were assembled to assess the fit of field data to model data, thereby serving as a method of comparative analysis to test the validity of the model. The profile of a selected cone can easily be constructed from a topographic map or a field photograph (after applying standard photogrammetric techniques for an approximate calibration). A variety of normalized profiles from the computer simulation can then be matched against the actual cone profile. Although a limitless number of profiles can be constructed, several examples of comparative profiles taken through the center of a cone are shown in Figs. 17–20. For this example the criterion for fit of the field profile to the model profile is empirical or 'best-fit' rather than statistical, although more

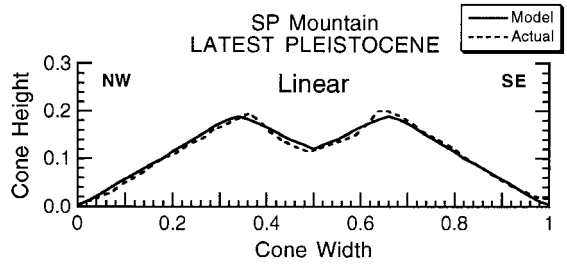

Fig. 17. The profile from an actual cone in a volcanic field can be fitted to a corresponding 'best-fit' normalized profile from the numerical simulation to assess the conformity of actual (or field) data to model data. This figure compares the fit of a profile from SP Mountain (V5703), a latest Pleistocene age cone in the San Francisco field (see Fig. 2a), to a normalized computer (or synthetic) profile generated by the linear diffusion-equation model at time step 400. The field profile of SP Mountain trends northwest–southeast. All profiles are displayed without vertical exaggeration. [The location of each cone is identified by a four-digit numbering system, as established by Moore and Wolfe (1987), Newhall et al. (1987), Ulrich and Bailey (1987), and Wolfe et al. (1987a,b). The first digit of the vent number represents the township (second digit of the township number), the second digit represents the range, and the last two digits are the section number in which the site is located.]

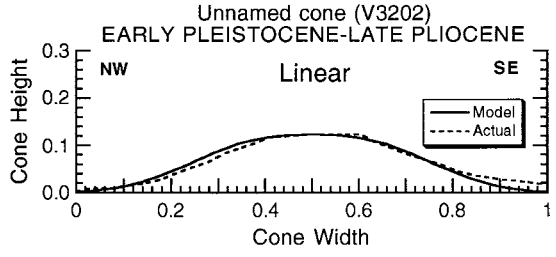

Fig. 18. This figure compares the fit of a profile of an unnamed cone (V3202) with an early Pleistocene–late Pliocene age in the San Francisco field (see Fig. 2b) to a normalized computer profile from time step 21,000 of the linear model.

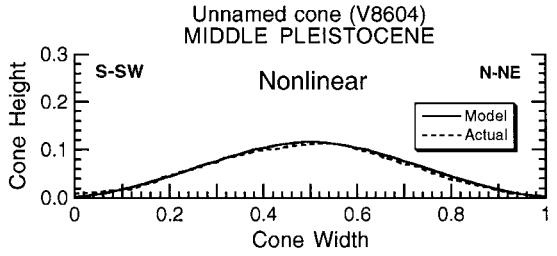

Fig. 19. This illustration compares the fit of a profile of an unnamed cone (V8604) with a middle Pleistocene age in the Springerville field to a normalized computer profile from time step 6500 of the nonlinear model.

mathematically rigorous methods could be selected. Most of the sets of normalized profiles exhibit a creditable fit with the largest discrepancy being the slight variation in crater morphology between examples of field and model cones. Other discrepancies can be attributed to the nonsymmetrical form of some cones due to the uneven dispersal of ejecta during their formation.

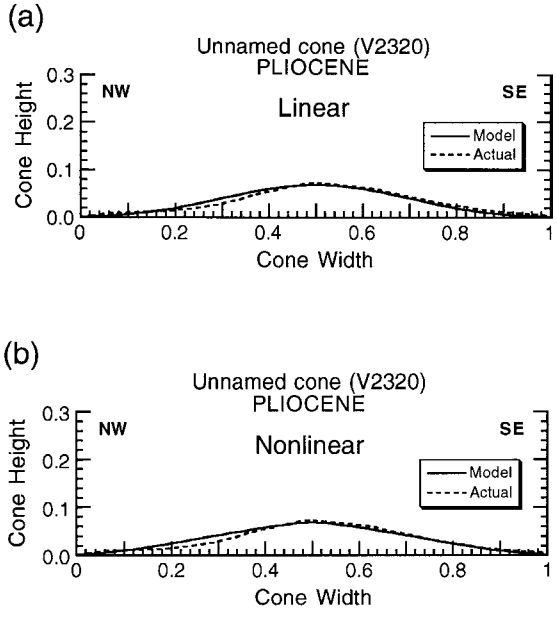

Fig. 20. This figure compares the fit of a profile of an unnamed cone (V2320) with a Pliocene age in the San Francisco field (see Fig. 2c) to a normalized computer profile from (a) the linear diffusion-equation model at time step 80,000 and (b) the nonlinear model at time step 25,000. There is a similarity in morphology at this stage, but the nonlinear model displays a more rapid erosion rate.

9. Comparative morphology and geomorphologic dating

The progressive changes in morphology and morphometry that a scoria cone experiences during erosion provide a basis for dating cones by a relative-age scheme or a relative-age scheme calibrated by radiometric dates. A variety of techniques can be employed to estimate the age of cones not dated by radiometric means. One example of dating cones of unknown stratigraphic age was devised by Wood (1980b). He plotted cone height versus cone width for 38 cones of assigned stratigraphic ages in the San Francisco volcanic field, AZ. Field studies by Moore et al. (1974, 1976) had produced informal age assignments ranging from Sunset (youngest) to Woodhouse (oldest at a maximum of 3 m.y.). Wood (1980b) then determined least-squares fits for H_{co}/W_{co} ratios of Sunset plus Merriam, Tappan, and Woodhouse ages. Then he analyzed the spread of each group to conclude that Sunset + Merriam age cones have H_{co}/W_{co} ratios greater than 0.15, the oldest Woodhouse age cones have H_{co}/W_{co} ratios less than 0.06, and Tappan age cones occupy the intermediate field. Finally, he plotted the H_{co}/W_{co} values of 28 cones of unknown stratigraphic age against these critical H_{co}/W_{co} lines to separate the cones into the same age groups. This method was applied to a pair of broad, poorly constrained cone age groups from the San Francisco volcanic field (cones not used in Table 1) in an attempt to provide more definitive age assignments (Hooper, 1994). While this technique is transferable to other fields, the least-squares values are not, mostly because of different erosion rates between volcanic fields.

Another approach was applied to 13 scoria cones in the Colima volcanic field, Mexico (Hooper, 1994; Hooper and Sheridan, 1994; Hooper, 1995). These cones have not yet been dated by radiometric methods, but a relative-age scheme was devised based upon their comparative morphology. The H_{co}/W_{co} ratio and maximum slope angle were determined for each cone, and the resulting values were then ranked or ordered. The sum of the rankings as well as the degree of crater erosion determined the relative-age placement (or geomorphologic dating) of the cones. Results from gully analysis were inconclusive, but this methodology incorporates most of the available

geomorphologic information. Using this simplistic scheme of morphology and morphometry, each cone was then placed into a relative-age group based on the spread of the geomorphologic parameters.

The ratio of crater depth to crater width (D_{cr}/W_{cr}) was observed in both field and simulation studies to decrease with increasing age. This indicates that the D_{cr}/W_{cr} parameter also has some usefulness as a relative indicator of age for a youthful group of cones (see Fig. 7). Normalized cone cross-sectional profiles (see Figs. 17–20) also offer another method to study progressive changes in morphology and to establish relative-age schemes, although they are not as reliable as other methods because of the variability that is possible with a slight change in profile direction.

10. Conclusion

We have quantitatively assessed the changing morphology of a series of temporally-distinct scoria cones in both the San Francisco and Springerville volcanic fields of Arizona. The degradational evolution of these cones can be correlated with the length of time they have been exposed to erosion. They exhibit a progressive decrease with increasing age in cone height/width ratio, maximum slope angle, average slope angle, and crater depth/width ratio.

A numerical model based on the diffusion-equation was used in a first-order attempt to simulate the degradational pattern witnessed in field observations and map measurements. The initial version of the model presented here was designed to simulate the erosion of an idealized, symmetrical scoria cone. We conclude that simulation results display a history of degradation that is comparable to that observed in field and map analysis. Variations in initial cone form, internal structure, weathering environment, welded or agglutinated layers, or external (secondary or non-erosional) modifications may produce some deviations in the morphologic parameters or in the general erosion pattern. Detailed fieldwork can reveal the extent of these variations, which is especially important if work concentrates upon a small number of cones, and then a modified erosional history can be constructed.

Comparative morphology can serve as a potentially useful dating tool for volcanic fields. A cone of unknown age can be loosely assigned an age by comparing the morphometric parameters of the cone in question with the spread of morphometric parameters occupied by a calibrated or dated group of cones from the same volcanic field. The accuracy and precision of these techniques does not permit them to replace absolute age data, but they can separate, for example, late Pleistocene scoria cones from early Pleistocene cones. Therefore, morphology-derived dating should always include an indication of the uncertainties or confidence of the age estimates (Mayer, 1987). The use of several morphometric or morphologic parameters is recommended when constructing any relative-age scheme.

The correlation of results from numerical modeling and field/map analyses provides the methodology to assess the rate of scoria cone degradation. The indicator of the rate of erosion is the diffusion coefficient. It is an empirical term, and thereby incorporates several assumptions and uncertainties. It is known to be a function of climate and lithology (e.g., Mayer, 1984; Andrews and Hanks, 1985; Pierce and Colman, 1986). We have presented values for the diffusion coefficient based on our study of the degradation of scoria cones (Table 4), but additional work remains to more clearly understand how and if the diffusion coefficient varies as a function of time, material properties (including lithology and particle size), vegetative covering, and climate. Wood (1980b) was perhaps the first to note that a study of cone morphology may offer information on past climates. There is uncertainty in reconstructing past climates, but it may be possible to correlate an increase in the erosion rate for certain cone age groups or subgroups with a possible increase in effective rainfall (Hooper, 1995). A combination of detailed chronometric data and a sufficient number of cones covering the desired time period would be required to identify any possible signature of an erosion cycle or climatic fluctuation (see Fig. 16).

We have concentrated our numerical approach on the two end-members of an erosion model in an effort to compare simulation results to actual field conditions. A review of both field/map and simulation results shows support for both linear and nonlinear transport models in these Arizona volcanic fields.

Many of the relatively older cones, such as those of Pliocene age, possess a concave hillslope (especially on the lower flanks) that can be approximated by a nonlinear transport law. For the more youthful Holocene and late Pleistocene cones, they often have crater rims and summit regions that are rounded as if they have been shaped by rainsplash or soil creep, processes characteristic of a linear transport law. The rims or summit regions of these younger cones can be expected to have a porous cinder mantle with a high infiltration capacity, whereas the lower flanks of an older cone may be dominated by overland flow (both channel and non-channel) and slope wash processes. Downslope transport on a scoria cone slope most likely encompasses several erosional processes that also vary in predominance during the lifespan of the cone. Further geomorphologic analyses would help to reveal the details of the complex hillslope processes responsible for the degradational evolution of these volcanic landforms.

Acknowledgements

The first author wishes to thank the agencies that supported the various aspects of this research, including the National Aeronautics and Space Administration (NASA) Graduate Students Researchers Program (NGT-50480/NGT-50691), NASA grant NAGW-2259 (to J. King), and a Guggenheim Postdoctoral Fellowship (National Air and Space Museum, Smithsonian Institution). The authors wish to thank C. Condit for providing a pre-print of the Springerville geologic map, T. Kover for writing the program for three-dimensional computer display, and M. Tuttle for assistance with image preparation and composition. The comments and suggestions provided by M. Bursik, P. Calkin, J. King, G. Valentine, and C. Wood are greatly appreciated. Reviews by E. Wolfe and S. Wells greatly improved the quality of this work.

References

Aguirre, E., Pasini, G., 1985. The Pliocene–Pleistocene boundary. Episodes 8, 116–120.

Andrews, D.J., Bucknam, R.C., 1987. Fitting degradation of shoreline scarps by a nonlinear diffusion model. J. Geophys. Res. 92, 12857–12867.

Andrews, D.J., Hanks, T.C., 1985. Scarp degraded by linear diffusion: Inverse solution for age. J. Geophys. Res. 90, 10193–10208.

Baksi, A.K., 1974. K–Ar study of the S.P. flow. Can. J. Earth Sci. 11, 1350–1356.

Bloomfield, K., 1975. A late-Quaternary monogenetic volcano field in central Mexico. Geol. Rundsch. 64, 476–497.

Breed, W.J., 1964. Morphology and lineation of cinder cones in the San Francisco volcanic field, Flagstaff, Arizona. Mus. North. Ariz. Bull. 40, 65–71.

Bursik, M., 1991. Relative dating of moraines based on landform degradation, Lee Vining Canyon, California. Quat. Res. 35, 451–455.

Carslaw, H.S., Jaeger, J.C., 1959. Conduction of Heat in Solids, 2nd edn. Oxford University Press, London, UK, 510 pp.

Carson, M.A., Kirkby, M.J., 1972. Hillslope Form and Process. Cambridge University Press, London, UK, 475 pp.

Chase, C.G., 1992. Fluvial landsculpting and the fractal dimension of topography. Geomorphology 5, 39–57.

Colman, S.M., 1987. Limits and constraints of the diffusion equation in modeling geological processes of scarp degradation. In: Crone, A., Omdahl, E. (Eds.), Directions in Paleoseismology, Proceedings of Conference XXXIX. U.S. Geol. Surv., Open-File Rep. 87–673, pp. 311–316.

Colman, S.M., Watson, K., 1983. Ages estimated from a diffusion equation model for scarp degradation. Science 221, 263–265.

Colton, H.S., 1967. The basaltic cinder cones and lava flows of the San Francisco volcanic field. (revised edition from 1936). Bull. Museum of Northern Arizona, Flagstaff, AZ, 58 pp.

Condit, C.D., 1991. Lithologic map of the western part of the Springerville volcanic field, east-central Arizona. U.S. Geol. Surv., Misc. Invest. Map I-1993, scale 1:50,000.

Condit, C.D., 1995. Dynamic digital map: The Springerville volcanic field. Boulder, CO, Geol. Soc. Am. Digital Publication Series DPSM01MC (CD-ROM for the Macintosh).

Condit, C.D., Connor, C.B., 1996. Recurrence rates of volcanism in basaltic volcanic fields: An example from the Springerville volcanic field, Arizona. Geol. Soc. Am. Bull. 108, 1225–1241.

Condit, C.D., Crumpler, L.S., Aubele, J.C., Elston, W.E., 1989. Patterns of volcanism along the southern margin of the Colorado Plateau: The Springerville volcanic field. J. Geophys. Res. 95, 7975–7986.

Condit, C.D., Crumpler, L.S., Aubele, J.C., in press. Geologic map of the Springerville volcanic field, east-central Arizona. U.S. Geol. Surv., Misc. Invest. Map I-2431, scale 1:100,000.

Connor, C.B., Condit, C.D., Crumpler, L.S., Aubele, J.C., 1992. Evidence of regional structural controls on vent distribution: Springerville volcanic field, Arizona. J. Geophys. Res. 97, 12349–12359.

Cooley, M.E., 1962. Geomorphology and the ages of volcanic rocks in northeastern Arizona. Ariz. Geol. Soc. Digest 5, 97–115.

Crank, J., 1975. The Mathematics of Diffusion, 2nd edn. Oxford University Press, London, UK, 414 pp.

Crowe, B.M., Perry, F.V., Turrin, B.D., Wells, S.G., McFadden, L.D., 1988. Volcanic hazard assessment for storage of high-level radioactive waste at Yucca Mountain, Nevada (Abstract). Geol. Soc. Am., Cordilleran Sect. 20, 153, Abstr. with Program.

Crowe, B., Turrin, B., Wells, S., McFadden, L., Renault, C., Perry, F., Harrington, C., Champion, D., 1989. Polycyclic volcanism: a common eruption mechanism of small volume basaltic volcanic centers of the southern Great Basin, USA (IAVCEI Abstract). N. Mex. Bur. Mines Miner. Resour. Bull. 131, 63.

Culling, W.E.H., 1960. Analytical theory of erosion. J. Geol. 68, 336–344.

Culling, W.E.H., 1963. Soil creep and the development of hillside slopes. J. Geol. 71, 127–161.

Culling, W.E.H., 1965. Theory of erosion on soil-covered slopes. J. Geol. 73, 230–254.

Damon, P.E., Shafiqullah, M., Leventhal, J.S., 1974. K–Ar chronology for the San Francisco volcanic field and rate of erosion of the Little Colorado River. In: Karlstrom, T.N.V., Swann, G.A., Eastwood, R.L. (Eds.), Geology of Northern Arizona, with Notes on Archaeology and Paleoclimate: Part 1, Regional Studies. Geol. Soc. Am., Rocky Mtn. Sect. Meeting, Flagstaff, AZ, pp. 221–235.

Dohrenwend, J.C., Wells, S.G., Turrin, B.D., 1986. Degradation of Quaternary cinder cones in the Cima volcanic field, Mojave Desert, California. Geol. Soc. Am. Bull. 97, 421–427.

Fick, A.E., 1855. Ueber diffusion. Ann. Phy. Chemie, Leipzig 94, 59–86.

Fourier, J.B.J., 1878. The Analytical Theory of Heat. Cambridge University Press, UK (Translated by Freeman, A., 1955. Dover Publishers, New York, 466 pp.).

Hanks, T.C., Bucknam, R.C., Lajoie, K.R., Wallace, R.E., 1984. Modification of wave-cut and faulting-controlled landforms. J. Geophys. Res. 89, 5771–5790.

Harbaugh, J.W., Bonham-Carter, G., 1970. Computer Simulation in Geology. Wiley, New York, 575 pp.

Hasenaka, T., Carmichael, I.S.E., 1985a. The cinder cones of Michoacán-Guanajuato, central Mexico: their age, volume and distribution, and magma discharge rate. J. Volcanol. Geotherm. Res. 25, 105–124.

Hasenaka, T., Carmichael, I.S.E., 1985b. A compilation of location, size, and geomorphological parameters of volcanoes of the Michoacán-Guanajuato volcanic field, central Mexico. Geofís. Int. 24, 577–607.

Hirano, M., 1968. A mathematical model of slope development: an approach to the analytical theory of erosional topography. J. Geosci., Osaka City University 11, 13–52.

Hodges, C.A., 1962. Comparative study of S.P. and Sunset Craters and associated lava flows. Plateau 35, 15–35.

Hooper, D.M., 1994. Geomorphologic modeling of the degradational evolution of scoria cones. PhD dissertation, State University of New York at Buffalo, Buffalo, NY, 312 pp.

Hooper, D.M., 1995. Computer-simulation models of scoria cone degradation in the Colima and Michoacán-Guanajuato volcanic fields, Mexico. Geofís. Int. 34, 321–340.

Hooper, D.M., Sheridan, M.F., 1994. Computer-simulation models of scoria cone degradation and the geomorphologic dating of scoria cones in the Colima volcanic complex, Mexico (Abstract). Volcán de Colima: 4th. International Meeting and Decade Volcano Workshop, Universidad de Colima, Colima, Mexico, Abstr. with Program, pp. 103–105.

Inbar, M., Hubp, J.L., Ruiz, L.V., 1994. The geomorphological evolution of the Paricutin cone and lava flows, Mexico, 1943–1990. Geomorphology 9, 57–76.

Kenyon, P.M., Turcotte, D.L., 1985. Morphology of a delta prograding by bulk sediment transport. Geol. Soc. Am. Bull. 96, 1457–1465.

Kirkby, M.J., 1971. Hillslope process-response models based on the continuity equation. Inst. Br. Geographers Special Pub. 3, 15–30.

Kover, T.P., 1995. Application of a digital terrain model for the modeling of volcanic flows: a tool for volcanic hazard determination. M.A. thesis, State University of New York at Buffalo, Buffalo, NY, 62 pp.

Luedke, R.G., Smith, R.L., 1978. Map showing the distribution, composition, and age of late Cenozoic volcanic centers in Arizona and New Mexico. U.S. Geol. Surv., Misc. Invest. Map I-1091-A, scale 1:1,000,000.

Luhr, J.F., Carmichael, I.S.E., 1981. The Colima volcanic complex, Mexico: Part II. Late-Quaternary cinder cones. Contrib. Mineral. Petrol. 76, 127–147.

Macdonald, G.A., 1972. Volcanoes. Prentice-Hall, Englewood Cliffs, NJ, 510 pp.

Martin del Pozzo, A.L., 1982. Monogenetic vulcanism in Sierra Chichináutzin, Mexico. Bull. Volcanol. 45, 9–24.

Mayer, L., 1984. Dating Quaternary fault scarps formed in alluvium using morphologic parameters. Quaternary Res. 22, 300–313.

Mayer, L., 1987. Sources of error in morphologic dating of fault scarps. In: Crone, A., Omdahl, E. (Eds.), Directions in Paleoseismology, Proceedings of Conference XXXIX, U.S. Geol. Surv., Open-File Report 87–673, pp. 302–310.

McGetchin, T.R., Settle, M., Chouet, B.A., 1974. Cinder cone growth modeled after Northeast Crater, Mount Etna, Sicily. J. Geophys. Res. 79, 3257–3272.

Moore, R.B., Wolfe, E.W., 1976. Geologic map of the eastern San Francisco volcanic field, AZ. U.S. Geol. Surv., Misc. Invest. Map I-953, scale 1:50,000.

Moore, R.B., Wolfe, E.W., 1987. Geologic map of the east part of the San Francisco volcanic field, north-central Arizona. U.S. Geol. Surv., Misc. Field Studies Map MF-1960, scale 1:50,000.

Moore, R.B., Wolfe, E.W., Ulrich, G.E., 1974. Geology of the eastern and northern parts of the San Francisco volcanic field, AZ. In: Karlstrom, T.N.V., Swann, G.A., Eastwood, R.L. (Eds.), Geology of Northern Arizona, with Notes on Archaeology and Paleoclimate: Part 1, Regional Studies, Geol. Soc. Amer., Rocky Mtn. Sect. Meeting, Flagstaff, AZ, pp. 465–494.

Moore, R.B., Wolfe, E.W., Ulrich, G.E., 1976. Volcanic rocks of the eastern and northern parts of the San Francisco volcanic field, Arizona. J. Res. U.S. Geol. Surv. 4 (5), 549–560.

Moretti, I., Turcotte, D.L., 1985. A model for erosion, sedimentation, and flexure with applications to New Caledonia. J. Geodyn. 3, 155–168.

Mosiño-Alemán, P.A., García, E., 1974. The climate of Mexico. In: Bryson, R.A., Hare, F.K. (Eds.), Climates of North America. Elsevier, Amsterdam, pp. 345–404.

Murray, A.B., Paola, C., 1994. A cellular model of braided rivers. Nature 371, 54–57.

Nash, D.B., 1980a. Forms of bluffs degraded for different lengths of time in Emmet County, Michigan, U.S.A. Earth Surf. Proc. 5, 331–345.

Nash, D.B., 1980b. Morphologic dating of degraded normal fault scarps. J. Geol. 88, 353–360.

Nash, D.B., 1984. Morphologic dating of fluvial terrace scarps and fault scarps near West Yellowstone, Montana. Geol. Soc. Am. Bull. 95, 1413–1424.

Newhall, C.G., Ulrich, G.E., Wolfe, E.W., 1987. Geologic map of the southwest part of the San Francisco volcanic field, north-central Arizona. U.S. Geol. Surv., Misc. Field Studies Map MF-1958, scale 1:50,000.

Pierce, K.L., Colman, S.M., 1986. Effect of height and orientation (microclimate) on geomorphic degradation rates and processes, late-glacial terrace scarps in central Idaho. Geol. Soc. Am. Bull. 97, 869–885.

Porter, S.C., 1972. Distribution, morphology, and size frequency of cinder cones on Mauna Kea volcano, Hawaii. Geol. Soc. Am. Bull. 83, 3607–3612.

Ray, R.G., 1960. Aerial photographs in geologic interpretation and mapping. U.S. Geol. Surv., Prof. Paper 373, 230 pp.

Renault, C.E., 1989. Hillslope processes on late Quaternary cinder cones of the Cima volcanic field, eastern Mojave Desert, CA. M.S. Thesis, University of New Mexico, Albuquerque, NM, 121 pp.

Renault, C.E., Wells, S.G., McFadden, L.D., 1988. Geomorphic and pedologic evidence for polygenetic volcanism in late Quaternary cinder cones: examples from Cima volcanic field, California and Crater Flat/Lathrop Wells volcanic field, Nevada (Abstract). Geol. Soc. Am. Annu. Meeting 20, 115, Abstr. with Program.

Reneau, S.L., Dietrich, W.E., Rubin, M., Donahue, D.J., Jull, J.T., 1989. Analysis of hillslope erosion rates using dated colluvial deposits. J. Geol. 97, 45–63.

Reynolds, S.J., 1988. Geologic map of Arizona. Arizona Geological Survey, Map 26, scale 1:1,000,000.

Richtmyer, R.D., Morton, K.W., 1967. Difference Methods for Initial-Value Problems, 2nd edn. Interscience Publishers (Wiley), New York, 405 pp.

Robinson, H.H., 1913. The San Francisco volcanic field. U.S. Geol. Surv., Prof. Paper 76, 213 pp.

Ruffner, J.A. (Ed.), 1985. Climates of the States, 3rd edn. Gale Research, Detroit, MI, 758 pp.

Scott, D.H., Trask, N.J., 1971. Geology of the Lunar Crater volcanic field, Nye County, NV. U.S. Geol. Surv., Prof. Paper, 599-I, 22 pp.

Segerstrom, K., 1950. Erosion studies at Parícutin, State of Michoacán, Mexico. U.S. Geol. Surv. Bull. 965-A, 164 pp.

Segerstrom, K., 1960. Erosion and related phenomena at Parícutin in 1957. U.S. Geol. Surv. Bull. 1104-A, pp. 1–18.

Segerstrom, K., 1966. Parícutin, 1965-Aftermath of eruption. U.S. Geol. Surv., Prof. Paper 550-C, pp. 93–101.

Sellers, W.D., Hill, R.H. (Eds.), 1974. Arizona Climate. The University of Arizona Press, Tucson, AZ, USA, 616 pp.

Settle, M., 1979. The structure and emplacement of cinder cone fields. Am. J. Sci. 279, 1089–1107.

Smiley, T.L., 1958. The geology and dating of Sunset Crater, Flagstaff, AZ. Ninth field conf., New Mexico Geol. Soc., field conf. guidebook, pp. 186–190.

Tanaka, K.L., Onstott, T.C., Shoemaker, E.M., 1990. Magnetostratigraphy on the San Francisco volcanic field, AZ. U.S. Geol. Surv. Bull. 1929, 35 pp.

Tanaka, K.L., Shoemaker, E.M., Ulrich, G.E., Wolfe, E.W., 1986. Migration of volcanism in the San Francisco volcanic field, Arizona. Geol. Soc. Am. Bull. 97, 129–141.

Turrin, B.D., Renne, P.R., 1987. Multiple basaltic eruption cycles from single vents, Cima volcanic field, California: evidence for polygenetic basaltic volcanism (Abstract). Geol. Soc. Am., Cordilleran Sect. 19, 458–459, Abstr. with Program.

Ulrich, G.E., Bailey, N.G., 1987. Geologic map of the SP Mountain part of the San Francisco volcanic field, north-central Arizona. U.S. Geol. Surv., Misc. Field Studies Map MF-1956, scale 1:50,000.

Wells, S.G., McFadden, L.D., Renault, C.E., Crowe, B.M., 1990. Geomorphic assessment of late Quaternary volcanism in the Yucca Mountain area, southern Nevada: implications for the proposed high-level radioactive waste repository. Geology 18, 549–553.

Wells, S., McFadden, L., Perry, F., Forman, S., Crowe, B., Poths, J., Olinger, C., 1992. Late Quaternary geology of small volcanic centers, SW USA: disparity among dating methods and implications for volcanic and geomorphic studies (Abstract). Geol. Soc. Am. Annu. Meeting 24, 102, Abstr. with Program.

Williams, H., McBirney, A.R., 1979. Volcanology. Freeman, Cooper & Co., San Francisco, 397 pp.

Wolfe, E.W., Ulrich, G.E., Holm, R.F., Moore, R.B., Newhall, C.G., 1987a. Geologic map of the central part of the San Francisco volcanic field, north-central Arizona. U.S. Geol. Surv., Misc. Field Studies Map MF-1959, scale 1:50,000.

Wolfe, E.W., Ulrich, G.E., Newhall, C.G., 1987b. Geologic map of the northwest part of the San Francisco volcanic field, north-central Arizona. U.S. Geol. Surv., Misc. Field Studies Map MF-1957, scale 1:50,000.

Wood, C.A., 1979. Monogenetic volcanoes of the terrestrial planets. Proc. 10th Lunar Planet. Sci. Conf., pp. 2815–2840.

Wood, C.A., 1980a. Morphometric evolution of cinder cones. J. Volcanol. Geotherm. Res. 7, 387–413.

Wood, C.A., 1980b. Morphometric analysis of cinder cone degradation. J. Volcanol. Geotherm. Res. 8, 137–160.